SCIENCE ▪ PASSION ▪ TECHNOLOGY

Small Angle Scattering
SAX(-ray)S / SAN(eutron)S

Heinz Amenitsch
TU-Graz & Austrian SAXS beamine, ELETTRA

Elettra Sincrotrone Trieste

fAnorganische CHEMIE

Layout

PART I: Introduction to SAS

- ❑ Introduction to the Theory (“Graz School”)
- ❑ From Experiments to Real Space
- ❑ Bio-SAXS (“Hamburg School”)

PART II: SAXS applications in life science and material science using synchrotron

- ❑ Examples: ▪ Chemistry
  ▪ Hierarchical Materials
- ❑ Grazing Incidence SAXS (“no school”)
  ▪ Biomembranes
  ▪ *In situ* Chemistry
- ❑ Some Aspects of Current Research

Soft Condensed Matter (© P. Schurtenberger)

3

Soft Matter - „complex fluids“ world between fluid and solid

Polymers

Length- and Timescales Contrasts

DNA

Block-copolymers

fd-Virus

Proteins

Colloids

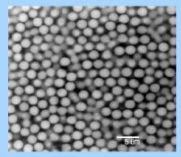

Surfactants

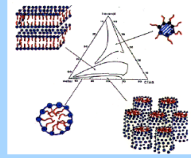

Equilibrium and Non-Equilibrium States

Characteristic length and time scales

(© P. Schurtenberger)

4

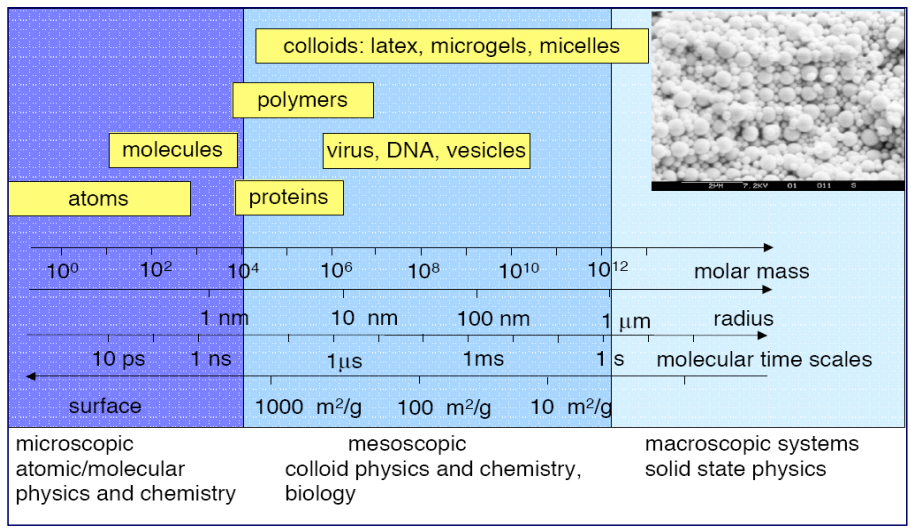

Research topics

5

ZnS NPs growth in a liquid jet

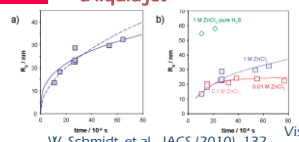

W. Schmidt, et al., JACS (2010), 132, 6822-6826

CdS nucleation and growth

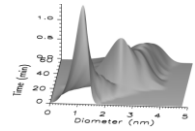

Viswanatha,R. *et al. J. Phys. Chem. Lett.* 1, 304 (2010)

Formation of mesoporous & crystalline materials

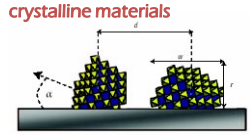

Grosso, D. et.al. *Nature Materials* 2004, *3*, 787-792.

Proteins

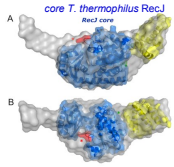

helical domain of the acyl-CoA

Krastanova I. et al. J. Biol. Chem. (2012)

Nanosystems

Mesostructured SiO_2 produced by aerosol reaction

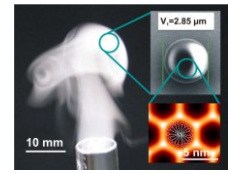

I.Shyjumon, et al., Rev.Scient.Instr., 79 (4), 043905 (2008), Langmuir (2011)

Biomechanics human arteries

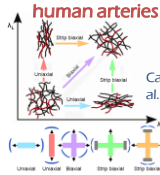

Cacho-Nerin, F., et al. (2015)

Biomembranes & drug delivery systems

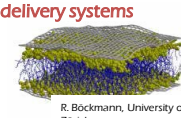

R. Böckmann, University of Zürich.

Rappolt M, Pabst G, Mariani et al.

SAXS and WAXS

6

SAXS and WAXS

7

Small – Angle : Supramolecular Envelope

Bragg's law:

$\sin \theta/2 = \lambda / 2d$

small θ large d

For CuK_α 0.154 nm (8 keV)

20 deg	0.5 nm
0.9 deg	10 nm
0.09 deg	100 nm

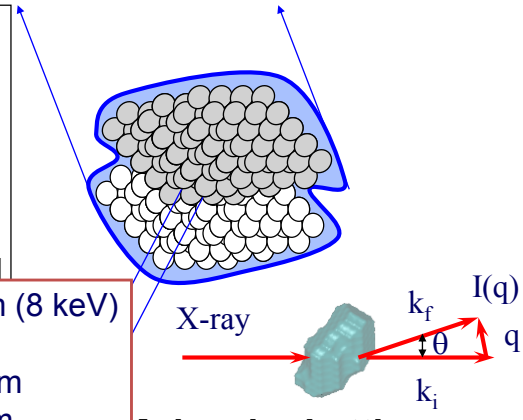

Molecular Lattice

The Scattered Field $E_s(q)$

8

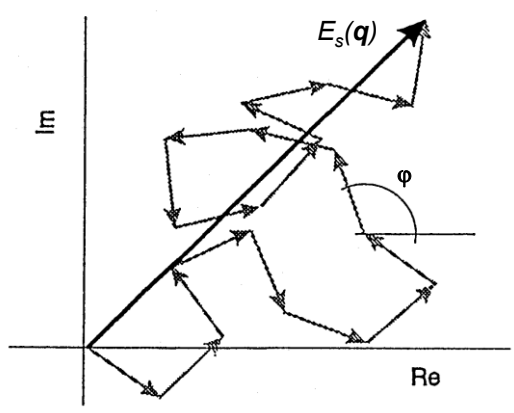

The scattering amplitudes of all coherently scattered waves have to be added according to their amplitude and relative phase $e^{i\varphi}$.

The phase difference depends on the relative location of the scattering centers.

The Phase Difference φ and the Scattering Vector $\boldsymbol{q}$

9

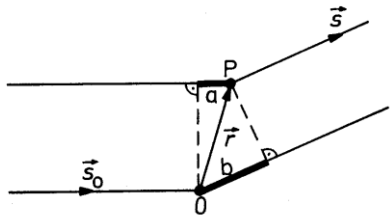

$$a = \vec{r} \cdot \vec{s}_0$$
$$b = \vec{r} \cdot \vec{s}$$

The path length difference is given by the length difference between the two paths a and b:

$$a - b = \boldsymbol{rs_0 - rs = -r(s-s_0)}$$

The phase difference φ is given by the wave number $(2\pi/\lambda)$ times the path length difference:

$$\varphi = -(2\pi/\lambda)\boldsymbol{r(s-s_0)}$$

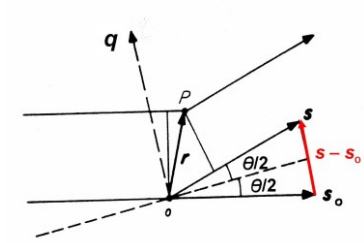

Now we introduce the scattering vector $\boldsymbol{q}$:

$$\boldsymbol{q} = (2\pi/\lambda)\boldsymbol{(s-s_0)} \rightarrow \boldsymbol{\varphi = -qr}$$

Its magnitude is:

$$q = 4\pi/\lambda \sin\theta/2$$

The Scattered Field $E_s(\boldsymbol{q})$

10

In order to find the total scattered field we have to integrate over the whole illuminated scattering volume *V*

$$E_s(\mathbf{q}) = const \int_V \rho(\mathbf{r})\, e^{-i\mathbf{qr}} d\mathbf{r}$$

We can now express the density $\rho(\boldsymbol{r})$ by its mean $\bar{\rho}$ and its fluctuations $\Delta\rho(\boldsymbol{r})$:

$$\rho(\mathbf{r}) = \bar{\rho} + \Delta\rho(\mathbf{r})$$

The Fourier integral is linear, so we can rewrite the above equation:

$$E_s(\mathbf{q}) = const\left[\int_V \bar{\rho} \cdot e^{-i\mathbf{qr}} d\mathbf{r} + \int_V \Delta\rho(\mathbf{r})\, e^{-i\mathbf{qr}} d\mathbf{r}\right]$$

Taking into account the large dimension of the scattering volume we get:

$$E_s(\mathbf{q}) = const \int_V \Delta\rho(\mathbf{r})\, e^{-i\mathbf{qr}} d\mathbf{r}$$

From Scattering Amplitudes to Scattering Intensities

11

For monodisperse dilute systems we can write:

$$I_s(q) = N < |E_1(\mathbf{q})|^2 > = N I_1(q)$$

We have introduced the single particle scattering amplitude $E_1(\mathbf{q})$ which is the scattered field resulting from integration over the particle volume only.

$$E_1(\mathbf{q}) = \int_V \Delta\rho(\mathbf{r})\, e^{-i\mathbf{qr}} d\mathbf{r}$$

$$|E_1(\mathbf{q})|^2 = E_1(\mathbf{q}) \cdot E_1^*(\mathbf{q}) = \int_V \int \Delta\rho(\mathbf{r}_1)\, \Delta\rho(\mathbf{r}_2)\, e^{-i\mathbf{q}(\mathbf{r}_1 - \mathbf{r}_2)} d\mathbf{r}_1\, d\mathbf{r}_2$$

We put $\mathbf{r}_1 - \mathbf{r}_2 = \mathbf{r}$ and use $\mathbf{r}_2 = \mathbf{r}_1 - \mathbf{r}$ and introduce the *convolution square* of the density fluctuations:

$$\gamma(\mathbf{r}) \equiv \Delta\tilde{\rho}^2(\mathbf{r}) = \int_V \Delta\rho(\mathbf{r}_1)\, \Delta\rho(\mathbf{r}_1 - \mathbf{r})\, d\mathbf{r}_1$$

The *Convolution Square* of the Density Fluctuations $\gamma(\mathbf{r})$ and $\gamma(r)$:

12

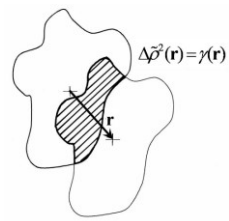

The function $\gamma(\mathbf{r})$ is calculated by shifting the "ghost" particle a vector $\mathbf{r}$ and integrating the overlapping volume.

This function is also called *spatial autocorrelation function (ACF)*.

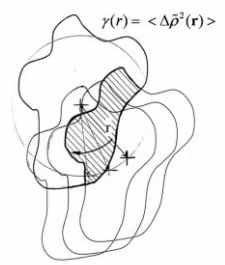

The spatially averaged convolution square γ(r) results from the same process, the ghost is shifted by a distance $r = |\mathbf{r}|$, but we have to average over all possible directions in space.

$$\gamma(r) = \int_V \Delta\rho(\mathbf{r}_1)\, \Delta\rho(\mathbf{r}_1 - \mathbf{r})\, d\mathbf{r}_1 >$$

SAXS and WAXS

13

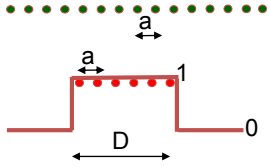

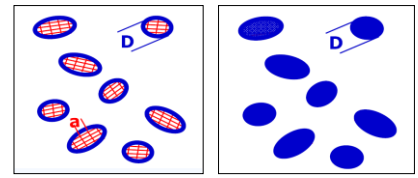

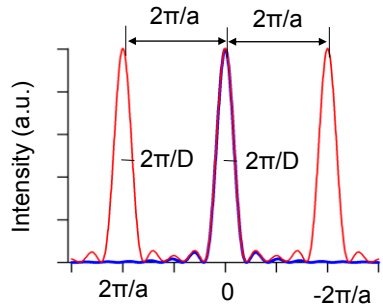

$$q = \frac{4\pi}{\lambda} \cdot \sin(\theta/2)$$

SAXS:
peak width (+ shape) → particle size

WAXS:
positions → lattice (type, spacings, strain)
width + shape → particle size
+ lattice strain fluctuations

RDG: Spatially Averaged Intensity *I(q)*

14

The spatially averaged intensity *I(q)* is given by:

$$I(q) = \langle |E_1(\mathbf{q})|^2 \rangle = \langle \int_V \Delta\rho \, e^{i\mathbf{q}\cdot\mathbf{r}} d\mathbf{r} \rangle$$

$$= 4\pi \int_0^\infty \gamma(r)\, r^2 \frac{\sin qr}{qr} dr$$

by introducing the *pair distance distribution function* (PDDF) *p(r)* with

$$p(r) = \gamma(r) \cdot r^2 = \Delta\rho \, r^2$$

we finally get

$$I(q) = 4\pi \int_0^\infty p(r) \frac{\sin(qr)}{qr} dr$$

The Scattering Problem and the Inverse Scattering Problem

15

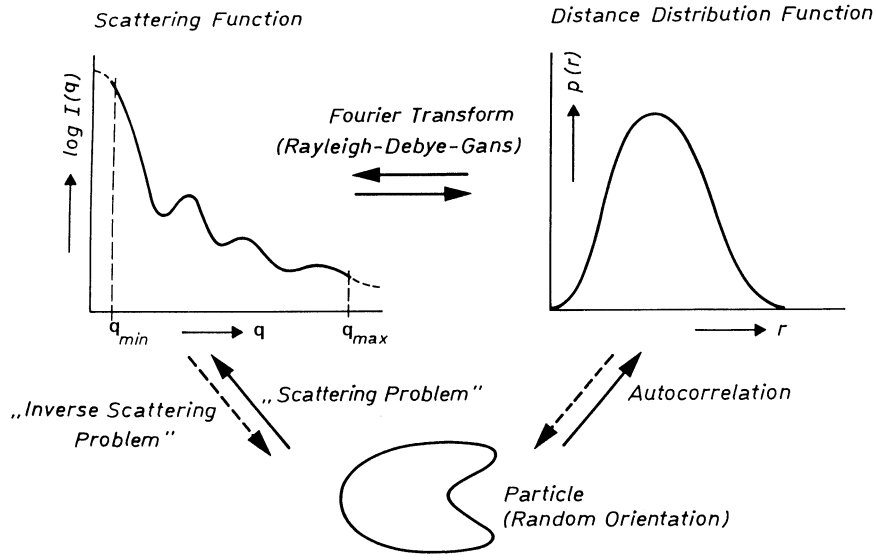

Definition of the *Pair Distance Distribution Function* (PDDF) *p(r)*

16

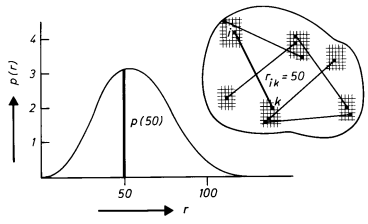

We can relate the meaning of a distance histogram to the PDDF *p(r)* if the particles are homogeneous. The height of *p(r)* is proportional to the number of distances that can be found inside the particle within the interval *r* and *r+dr*

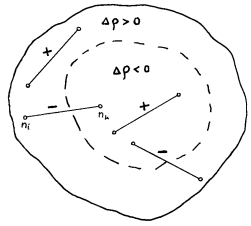

The *p(r)* function of inhomogeneous particles is proportional to the product of the difference scattering lengths $n_i n_k$ [$n_i = \Delta\rho(\mathbf{r}_i)dV(\mathbf{r}_i)$] of two volume elements *i* and *k* with a center-to-center distance between *r* and *r+dr* and we sum over all pairs with this distance.

Inverse Problem in Scattering – Artists View*

17

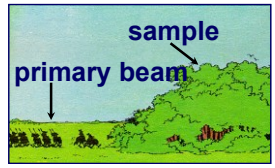

design of the experiment

*** "Asterix in Belgium"**

associated by Anna Stradner & Gerhard Fritz

result in q-space

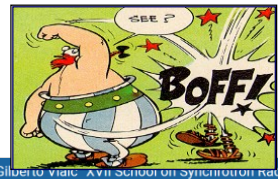

?

structure of the scattering particle

RDG: The Particle Form Factor

18

$$I_s(q) = NI_1(q) = NI_1(0)P(q)$$

$I_1(0) = V^2\Delta\rho^2$ intensity of single particle at q = 0

$P(q)$ particle form factor, where

$$P(q) = \frac{I_1(q)}{I_1(q \to 0)}$$

The normalized form factor *P(q)* contains information about size and structure of the particle.

Form factor of a homogeneous sphere:

$$P(q) = \left[\frac{3(\sin qR - qR\cos qR)}{(qR)^3}\right]^2$$

The Particle Form Factor

19

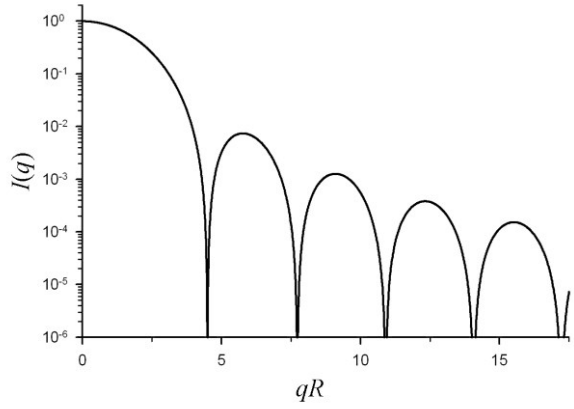

The function has minima for tan(qR) = qR, or qR = 4.49, 7.73, …

Different Shapes of Homogeneous Particles

20

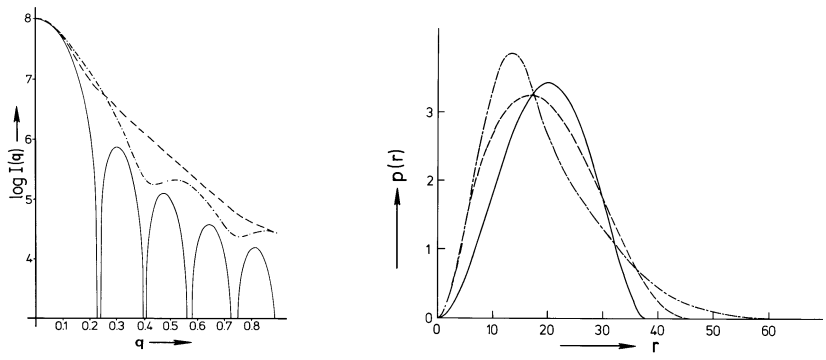

Comparison of a sphere (full line) an oblate ellipsoid (dashed line) and a prolate ellipsoid with the same volume.

Rod-like Particles

21

Let us regard a rod of length L and of cross-section A_c = The cross-section A_c (with maximum dimension d) should be small in comparison to the length of the whole particle L (d<<L). For $q > 1/L$ we can write

$$I(q) = \frac{L\pi}{q} \cdot I_c(q)$$

The cross-section scattering function $I_c(q)$ is related to the cross-section distance distribution $p_c(r)$ by

$$I_c(q) = 2\pi \int_0^\infty p_c(r) J_0(qr)\, dr$$

where

$$p_c(r) = \gamma_c(r) \cdot r = 2\pi r \int_{Ac} \Delta\rho_c(r') \Delta\rho_c(r'+r)\, dr$$

Scattering Function for a Long, Rod-like Particle Schematic Representation

22

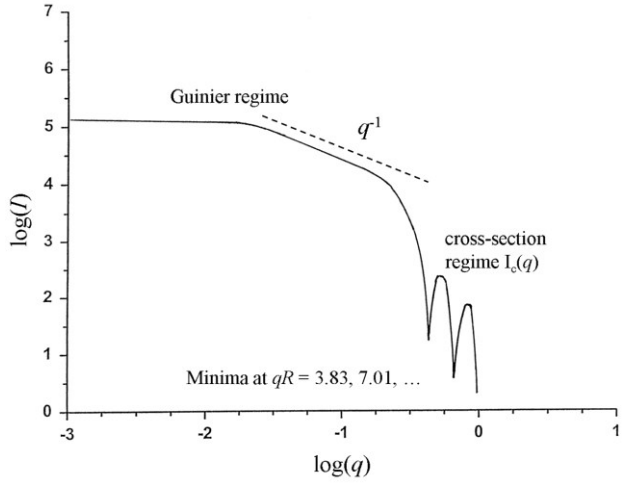

The different regimes can be visualized is a *log(I)* vs. *log(q)* plot of the scattering curve:

The Guinier regime, the q^{-1} regime and the cross-section regime.

PDDF's for Rod-like Particles

23

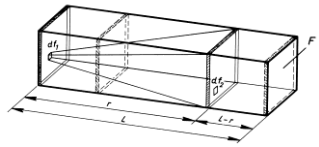

$$p(r) = \frac{2}{4\pi} \int_r^L \int_A \int_A \Delta\rho^2 df_1\, df_2\, dx = \frac{1}{2\pi} \Delta\rho^2 A_c^2 (L - r),$$

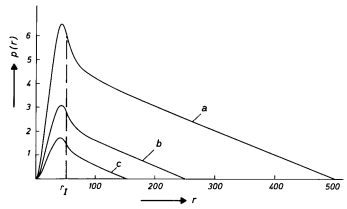

PDDF from homogeneous prisms with edge lengths of: (a) 50:50:500, (b) 50:50:250 and (c) 50:50:150

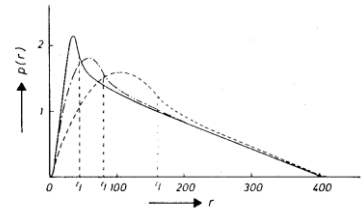

PDDF for three parallel epipeds with constant length L (400 Å) and constant cross-section area A_c but varying length of the edges: 40:40, -∢-∢- 80:20 and ----- 160:10.

Flat Particles

24

Let us now consider a flat particle, with a finite and constant thickness D_t, being extremely large in the two other dimensions with an area A. In full analogy to the case of the rod we can separate the scattering amplitude into a *planar factor* $2\pi Aq^{-2}$ and a *thickness-factor* $I_t(q)$, i.e. the total intensity is given by

$$I(q) = I_{plane} \cdot I_t(q) = \frac{2\pi A}{q^2} \cdot I_t(q).$$

The thickness-factor is related to the thickness distance distribution $p_t(r)$ by

$$I_t(q) = 2 \int_0^\infty p_t(r) \cos(qr)\, dr$$

where

$$p_t(r) = \gamma_t(r) = 2 \int_0^\infty \Delta\rho_t(r') \Delta\rho(r' + r)\, dr.$$

Scattering Function for a Flat, Lamellar Particle. Schematic Representation

25

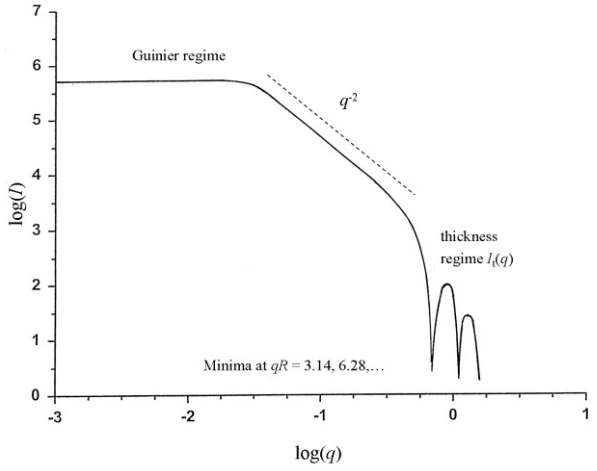

The different regimes can be visualized is a *log(I)* vs. *log(q)* plot of the scattering curve:

The Guinier regime, the q^{-2} regime and the thickness regime.

PDDF's for Flat Particles

26

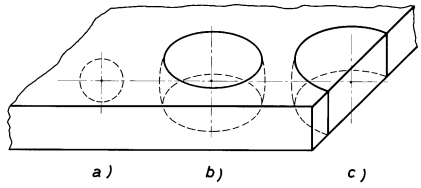

Sketch for the qualitative discussion of the PDDF of a flat particle

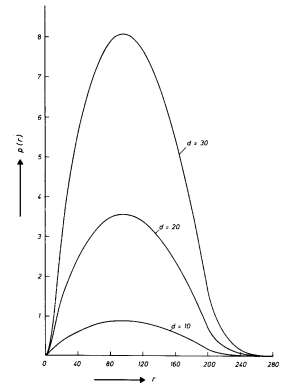

PDDFs of lamellar particles with the same basal plane (200 x 200Å) and different thickness D_t: (a) D_t = 10Å, (b) D_t = 20Å and (c) D_t = 30Å.

Inhomogeneous Particles: Spheres and Cylinders with Radial Inhomogeneity

27

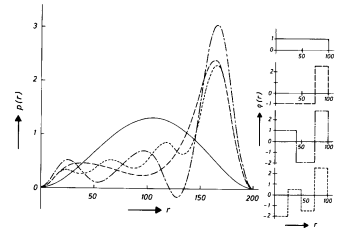

Spherical multilayer models with constant outer diameter of 200 Å. PDDFs in the left part, density profiles in the right part of the figure.

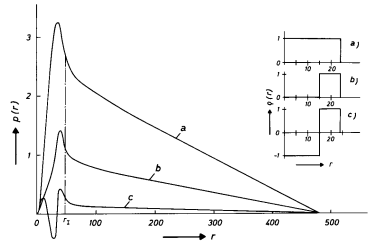

Circular cylinders with a constant length of 480 Å and an outer diameter D_c of 48 Å. (a) Homogeneous cylinder, (b) hollow cylinder, (c) inhomogeneous cylinder. The PDDFs are shown on the left, the corresponding radial density distributions $\rho(r)$ on the right.

Aggregates - Dimers

28

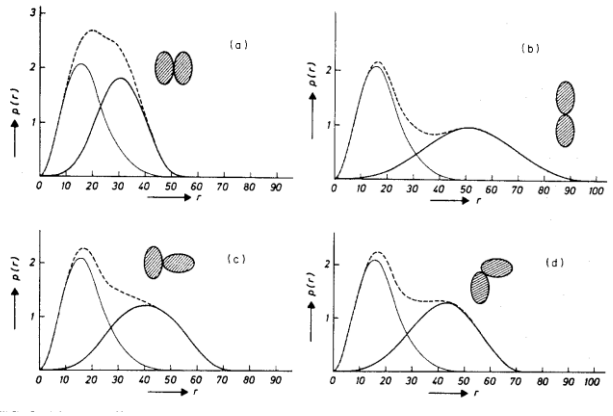

PDDFs from dimer models built from prolate ellipsoids. Monomers (full line), dimers (broken line), and difference between dimers and monomers (thick full line).

Polydisperse Systems

29

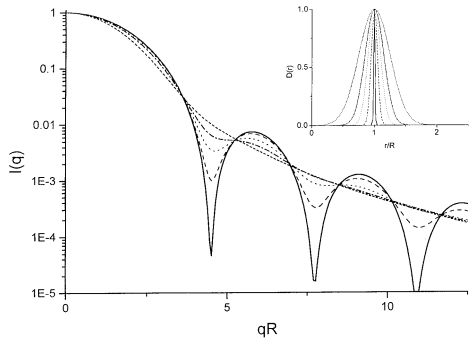

Intensity Distribution

$$I(q) = c_i \int_0^\infty D_i(R) \cdot P_0(q,R)\, dR$$

Volume or Mass Distribution

$$I(q) = c_v \int_0^\infty D_v(R) \cdot R^3 \cdot P_0(q,R)\, dR$$

Number Distribution

$$I(q) = c_n \int_0^\infty D_n(R)\, R^6 \cdot P_0(q,R)\, dR$$

Scattering curves of Gaussian size distributions of spheres with varying width (see inset).

Radius of Gyration

30

The radius of gyration is one of the most important parameters in the field of small-angle scattering. In full analogy to the radius of intertia in mechanics it is defined as

$$R_g^2 = \frac{\int \Delta\rho(r_1)\, r_i^2\, dV_i}{\int \Delta\rho(r_i)\, dV_i}$$

According to the momentum theorem of Fourier transformation the second moment of a function in one space is related to the second derivative (curvature) of its Fourier transform at the origin. This relation is the basis of the so-called *Guinier approximation* for the description of *I(q)* for low *q* derived from a series expansion:

$$I(q) = I(0)\, e^{-\frac{q^2 Rg^2}{3}}$$

We can also use another relation for the estimation of the radius of gyration:

$$R_g^2 = \frac{\int p(r)\, r^2\, dr}{2\int p(r)\, dr}$$

Radius of Gyration - Guinier Plot

31

From the previous equation it is clear that we can calculate the radius of gyration from the PDDF once it is known. Otherwise we can use the Guinier approximation to determine R_g directly from the scattering data with a so-called *Guinier-plot*.

Plotting *ln (I(q)) vs* q^2 we get a straight line with a slope proportional to R_g^2.

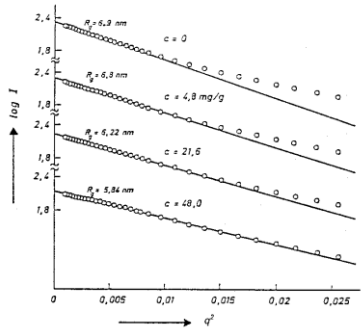

Example for a Guinier plot from scattering data of a protein solution with varying concentration, including an extrapolation to zero concentration.

Radius of Gyration of the Cross-Section

32

For rod-like particles we can also define a radius of gyration of the cross-section which can be calculated from $p_c(r)$ by

$$R_c^2 = \frac{\int p_c(r)\, r^2\, dr}{2\int p_c(r)\, dr}$$

or it can be estimated in reciprocal space form

$$I_c(q) = I_c(0)\, e^{-\frac{q^2 R_c^2}{2}}$$

by a so-called cross section Guinier plot *[log(I(q)q) vs.* q^2*]*.

Radius of Gyration of the Thickness Function

33

For lamellar particles we can also define a radius of gyration of the thickness function which can be calculated from $p_t(r)$ by

$$R_t^2 = \frac{\int p_t(r)\, r^2\, dr}{2\int p_t(r)\, dr}$$

or it can be estimated in reciprocal space form

$$I_t(q) = I_t(0)\, e^{-q^2 R_t^2}$$

by a so-called thickness Guinier plot *[log(I(q)q²) vs. q²].*

Porod Limit - Porod Plot - Fractals

34

We proceed now to the discussion of the **final slope** of the scattering curve at high *q*-values, we may expect this to depend mainly on the fine structure of the particle.

$$I(q)_{q\to\infty} = (\Delta\rho)^2 \cdot \frac{2\pi}{q^4} \cdot S$$

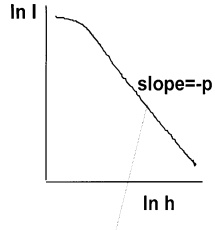

1-2 decades

For mass fractals,where
$1 < D < 3$, and $M \propto R^D$
it holds, that
$p = D$

For **surface** fractals, where
$2 < D_s < 3$
it holds, that
$p = 6 - D_s$

Contrast Variation: Index Match

35

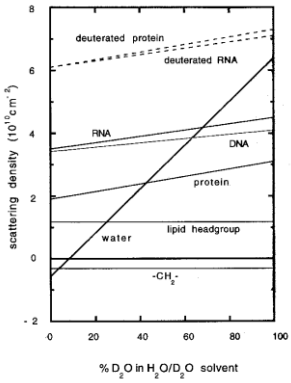

A mixture of H2O and D2O allows to match different regions in a sample.

When the monster came, Lola, like the peppered moth and the arctic hare, remained motionless and undetected, Harold, of course, was immediately devoured!

Autrans'94 R. May (found in „Los Alamos Science")

Contrast Variation in SAXS by Anomalous Scattering

36

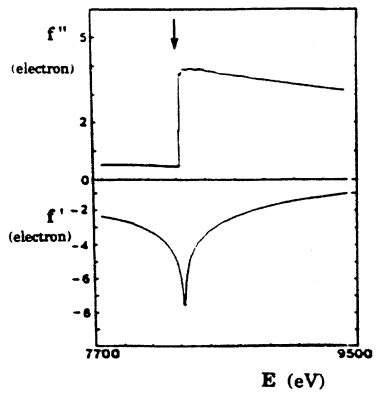

Typical energy dependence of f' and f'' near the absorption edge of an element. Shown here is the nickel *K* edge at 8333 eV.

This method, also known as *resonant small angle scattering* uses another possibility for the variation of the contrast. Near the inner shell absorption edge, the coherent scattering length or atomic scattering factor of an atom is a function of the energy *E* of the X-ray photon:

$$f(E) = Z + f'(E) + if''$$

Energy variation is only possible with the "white" X-ray beam of a synchrotron. The main problem for applications in chemistry is the fact that the edges for *C, H, N* and *O* are outside the useful energy window at very low energies. In solution experiments this effect might be useful for heavy counter ions (Br^+) in micellar systems.

The Scattering Problem and the Inverse Scattering Problem

37

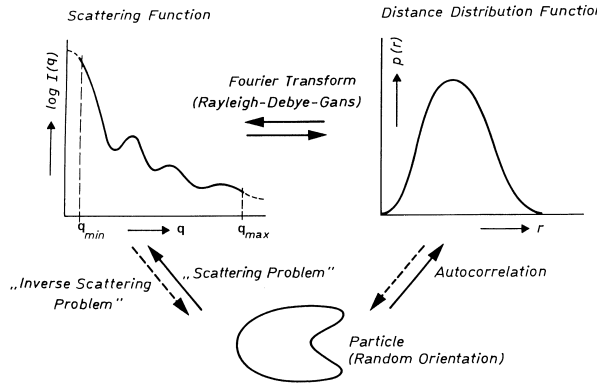

For the solution of the inverse Problem it is essential to be able to calculate the PDDF form the experimental scattering curve with minimum termination effect.

From experimental data to the PDDF

38

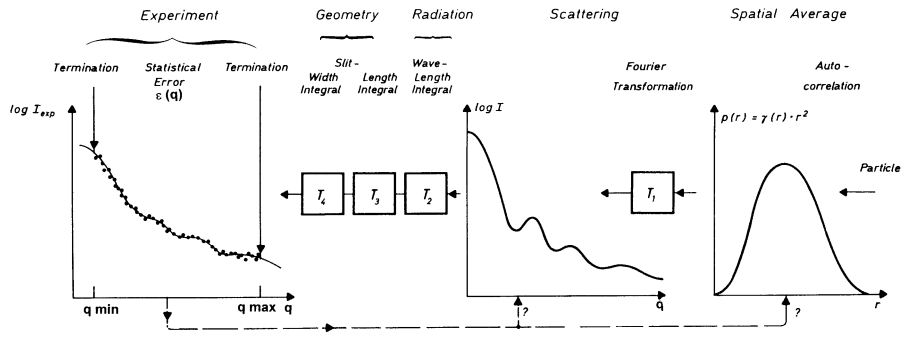

All Transformations T1 to T4 are linear and are mathematically well defined, this does not hold for their inverse transformations.

The Principles of the Indirect Fourier Transformation

39

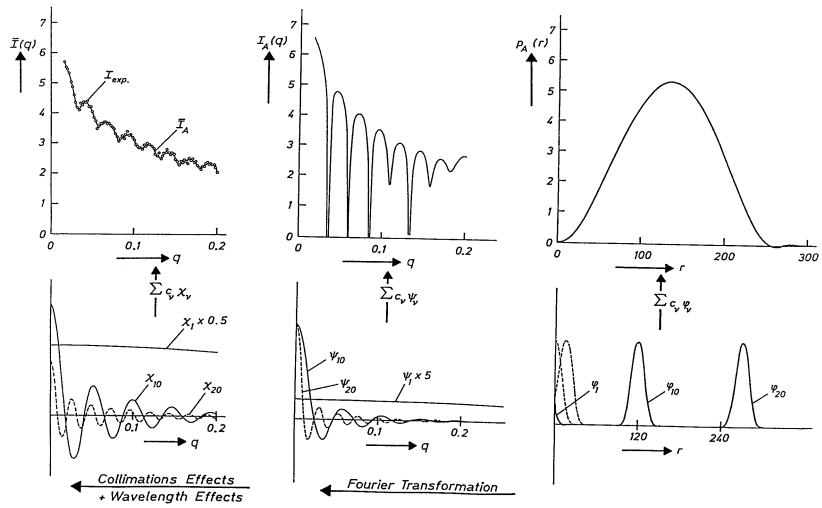

Other IFT Applications - Equations

40

Summary of the different transforms T_1 used in *IFT*:

Arbitrary shape:

$$I(q) = 4\pi \int_0^\infty p(r) \frac{\sin(qr)}{qr} dr$$

Cylindrical Symmetry:

$$I(q) = \frac{2\pi^2 L}{q} \int_0^\infty p_c(r) J_0(qr) dr$$

Lamellar Symmetry:

$$I_{plane}(q) = \frac{4\pi A}{q^2} \int_0^\infty p_t(r) \cos(qr) dr$$

The structure is the same for all equations, just the kernels of the integrals differ!

Deconvolution of the PDDF – The *Magic Square*

41

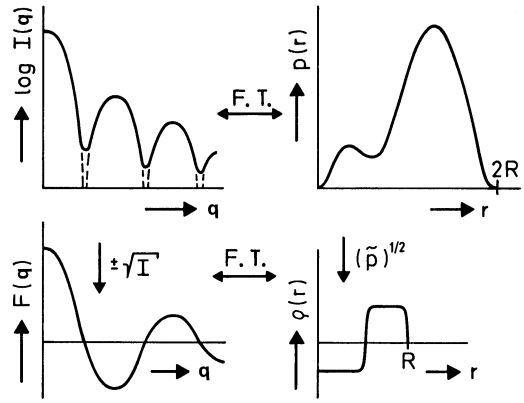

The *Magic square* of small-angle scattering: The correlations between the radial density $\Delta\rho(r)$ and the PDDF $p(r)$ and their Fourier transforms, the scattering amplitude $F(q)$ and scattering intensity $I(q)$ under the assumption of spherical symmetry.

Deconvolution of the PDDF – Principles I

42

Here we are facing a similar situation as in the *IFT* method: for a given density distribution $\rho(r)$ we can calculate the exact $p(r)$-function for all three cases (spherical, cylindrical and lamellar symmetry) by a convolution square operation but we do not have a useful description of the inverse problem, the so-called convolution square root.

As an additional problem we have to keep in mind the fact, that the convolution square operation is a **nonlinear transformation** which will not allow an inversion by the solution of a simple linear least squares technique like in the case of the indirect Fourier transformation.

We start again with a series expansion of the radial density function $\rho(r)$ in the usual way:

$$\bar{\rho}(r) = \sum_{i=1}^{N} c_i \, \varphi_i(r)$$

Deconvolution of the PDDF – Principles II

43

The approximation for the density profile corresponds to an approximation to the PDDF:

$$\bar{p}(r) = \sum_{i=1}^{N} V_{ii}(r)\, c_i^2 + 2 \sum_{i>k} V_{ik}(r)\, c_i\, c_k$$

The overlap integrals $V_{ik}(r)$ describe the overlapping of the *i-th* with the *k-th* step or shell where one function has been shifted an arbitrary distance *r*. These overlap or convolution integrals are very simple for the planar case (one-dimensional convolution of two step function leads simply to a triangle) but are a bit more complicated for the cylindrical and spherical case:

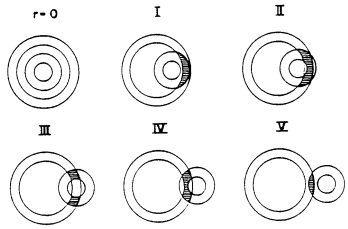

Illustration of the five sub-regions for the calculation of the overlap integrals $V_{ik}(r)$.

Deconvolution of the PDDF – Iterative Solution

44

The above equation for the PDDF is nonlinear in its coefficients c_i. The corresponding least squares problem has to be linearized by a series expansion where higher order terms are omitted.

Such linearized systems must be solved iteratively. In addition one needs starting values $c_i^{(0)}$ for the first iteration. Here we set all coefficients equal to a constant.

We then calculate the difference function

$$\Delta p(r) = p(r) - \bar{p}^{(o)}(r)$$

which would be zero only if we would know the exact coefficients c_i.

Now we calculate correction terms Δc_i in order to minimize $\Delta p(r)$ in a least square sense.

$$\sum_{i=1}^{N} V_{ii}(r)\left[\left(c_i + \Delta c_i\right)^2\right] + 2\sum_{i>k} V_{ik}(r)\left[\left(c_i + \Delta c_i\right)\left(c_k + \Delta c_k\right) - c_i c_k\right] = \Delta p(r)$$

Deconvolution of the PDDF – Iterative Solution II

45

We linearize this equation by omitting the second order terms Δc_i^2 and $\Delta c_i \Delta c_k$ and we get

$$2\sum_{k=1}^{N}\sum_{i=1}^{N} c_i V_{ik}\left(r_j\right)\Delta c_k = \Delta p\left(r_j\right)$$

for $j = 1,2,3,\ldots M$ and $M > N$. These equations can be written in matrix notation

$$A_{jk}\Delta c_k = \Delta p_j \quad \text{or} \quad \mathbf{A}\Delta\mathbf{c}^{(0)} = \Delta\mathbf{p}^{(0)}$$

where the matrix elements A_{jk} are given by

$$A_{jk} = 2\sum_{i=1}^{N} c_i V_{ik}\left(r_j\right)$$

This system is solved with a weighted least squares condition considering the standard deviations of the function $\Delta p(r)$ and we get the correction terms $\Delta\mathbf{c}$.

Deconvolution of the PDDF – Iterative Solution III

46

They allow the calculation of improved coefficients $c_i^{(1)}$:

$$c_i^{(1)} = c_i^{(0)} + \Delta c_i$$

and with these coefficients we start the next iteration, get further improvements and if this iterative procedure converges we have solved the problem.

This problem is, however, again an *ill-posed problem* so that we have to add again a stabilization criterion and we have to solve the nonlinear problem by iteration for every *Lagrange multiplier*.

Many applications performed in the meantime have shown that the deconvolution technique works well in combination with the indirect transformation method, also in cases where the conditions of symmetry are not perfectly fulfilled.

"Gilberto Vlaic" XVII School on Synchrotron Radiation: Fundamentals, Methods and Applications
amenitsch@tugraz.at & amenitsch@elettra.trieste.it
Anorganische CHEMIE

Surfactant Systems - Spherical micelles

47

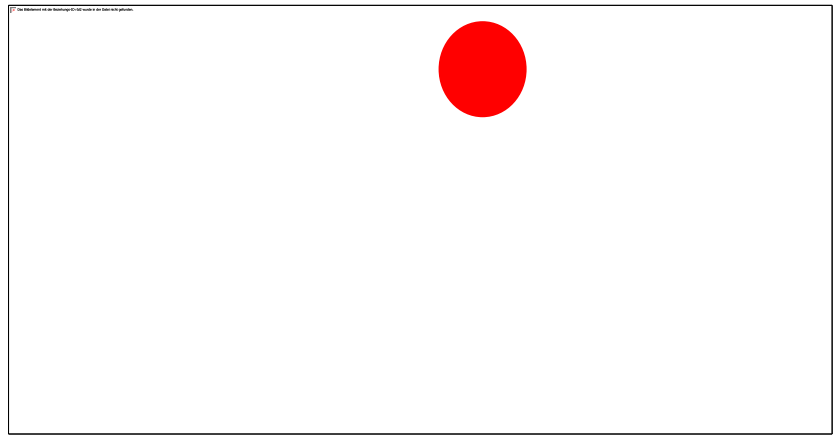

Scattering pattern of spherical aggregates with radius *R*. The scattering curve *I(q)* is the Fourier transform of the PDDF *p(r)*. This PDDF is the convolution square of the radial density distribution $\Delta\rho(r)$.

SAXS 2.0: Theoretical Background

48

Assumption of monodisperse globular particles:

$$I(q) = n.P(q).S(q)$$

n ... Particle density
q ... Scattering vector
I(q) ... Scattering Intensity
P(q) ... Form Factor $P(q) \leftrightarrow p(r)$
S(q) ... Structure Factor $[S(q) - 1] \leftrightarrow [g(r) - 1]$
Interaction Potential: Hard Spheres Potential
Closure relation: Percus-Yevick-Approximation (analyt. Solution)
Kinning & Thomas, *Macromolecules* (1984), **17**

Fourier Transformation

49

$$I(q) = n.P(q).S(q)$$

Form Factor $P(q)$ ↔ Pair Distance Distribution Function $p(r)$

$$P(q) = 4\pi \int_0^\infty [\quad] \frac{\sin(qr)}{qr} dr$$

Structure Factor [$S(q)$ - 1] ↔ Total Correlation Function [$g(r)$ -1] r^2

$$S(q) - 1 = 4\pi \int_0^\infty [\quad] \frac{\sin(qr)}{qr} dr$$

Due to the nearly identical structure of these equations it is obvious that it is not a trivial task to split the scattering intensity into these factors by mathematical means

GIFT (=General Indirect Fourier Transformation)

ATSAS Package

50

D.Svergun Hamburg Group

General principle of SAS modelling

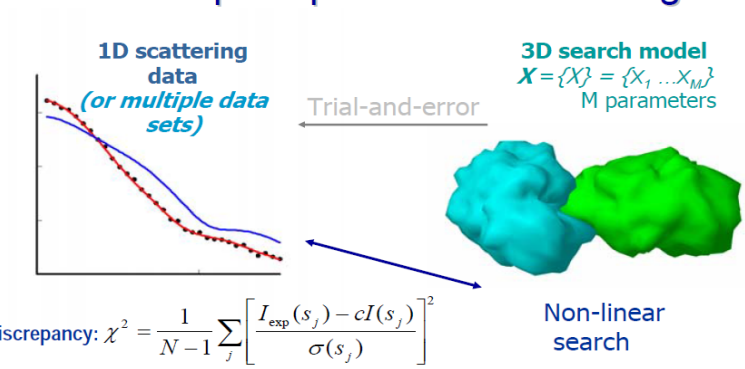

Additional information is ALWAYS required to resolve or reduce ambiguity of interpretation at given resolution

Constraints and Restraints

51

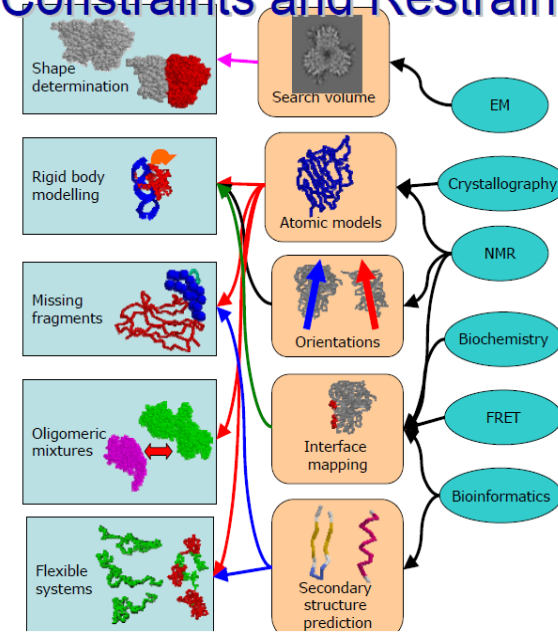

52

Target function

- To reduce the ambiguity of data analysis

$$E(\{X\}) = \chi^2[(I(s), I_{\exp}(s)] + \sum_i \alpha_i P_i$$

is minimized

- Penalties describe model-based restraints and/or introduce the available additional information from other methods: MX, NMR, EM etc)
- If the number of free parameters is small, a brute force (grid) search may be applied, otherwise a Monte-Carlo based technique (e.g. simulated annealing) is employed to perform the minimization of *E({X})*

53

Ab initio shape determination

A sphere of radius D_{max} is filled by densely packed beads of radius $r_0 << D_{max}$

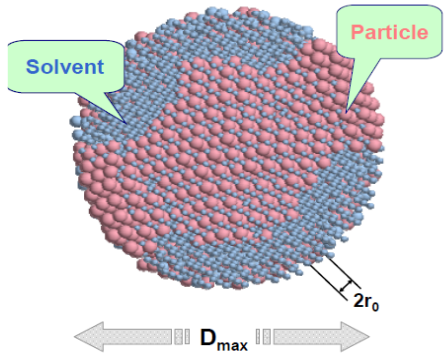

Vector of model parameters:

Position (j) = X_j = { 1 if particle / 0 if solvent

(phase assignments)

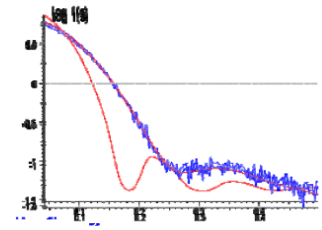

Svergun, D.I. (1999) ***Biophys. J.*** 76, 2879-2886

54

Bead Modelling: DAMMIN

- Scattering intensity is computed using spherical harmonics

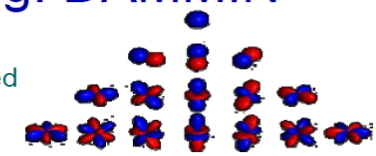

$$A_{lm}^{(k)}(s) = i^l \sqrt{2/\pi}\, f(s) \sum_{j=1}^{N_k} j_l(sr_j)\, Y_{lm}^*(\omega_j)$$

$$I(s) = 2\pi^2 \sum_{l=0}^{\infty} \sum_{m=-l}^{l} \left\{ \sum_{k=1}^{K} \left[\Delta\rho_k A_{lm}^{(k)}(s)\right]^2 + 2 \sum_{n>k} \Delta\rho_k A_{lm}^{(k)}(s) \Delta\rho_n \left[A_{lm}^{(n)}(s)\right]^* \right\}$$

- Penalty terms ensure compactness and connectivity

compact

loose

disconnected

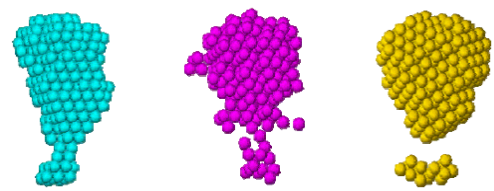

Svergun, D.I. (1999) ***Biophys. J.*** 76, 2879-2886

Scattering on human CDC45 Protein

55

CDC45 protein conserved in all eukaryotes
initiation of DNA replication
progression of the replication fork

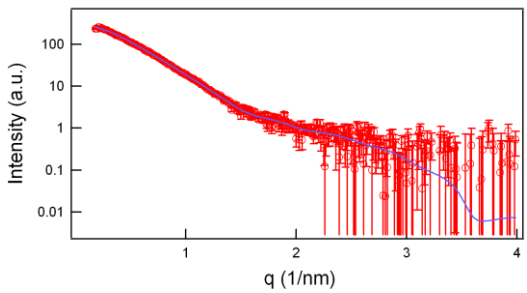

hCDC45, 1.85 mg/ml, 40µl, 30 s

Kastranova I, Onesti S et al.,J.Biol.Chem. (2012)

core T. thermophilus RecJ

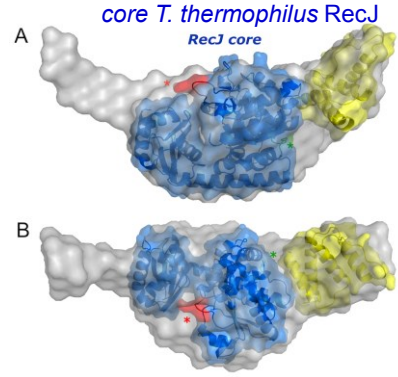

helical domain of the acyl-CoA

56

Multiphase bead modelling

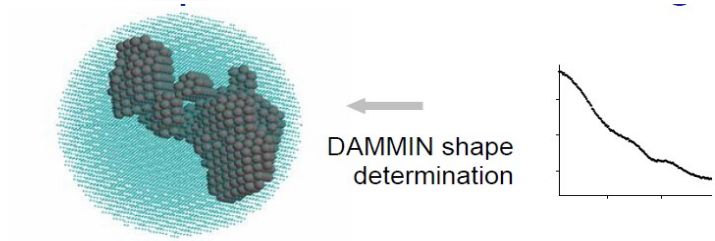

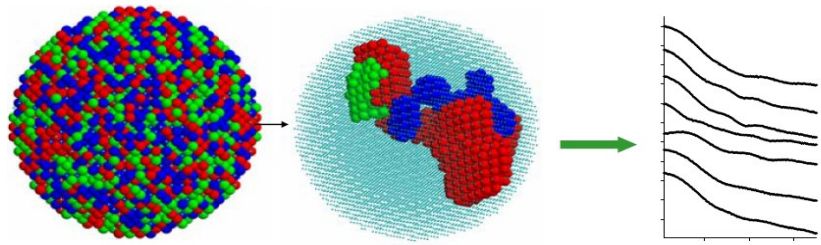

- One can differentiate between distinct parts of the particle
- Several curves are fitted assuming the same arrangement of the parts in different samples

57

How to compute SAS from atomic model

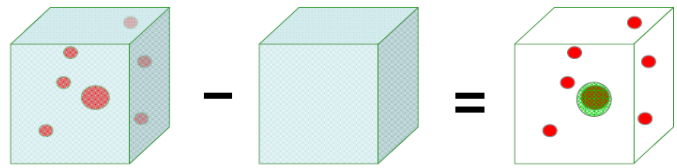

$I_{solution}(s)$ $I_{solvent}(s)$ $I_{particle}(s)$

- To obtain scattering from the particles, solvent scattering must be subtracted to yield effective density distribution $\Delta\rho = <\rho(\mathbf{r}) - \rho_s>$, where ρ_s is the scattering density of the solvent
- Further, the bound solvent density may differ from that of the bulk

58

Scattering from a macromolecule in solution

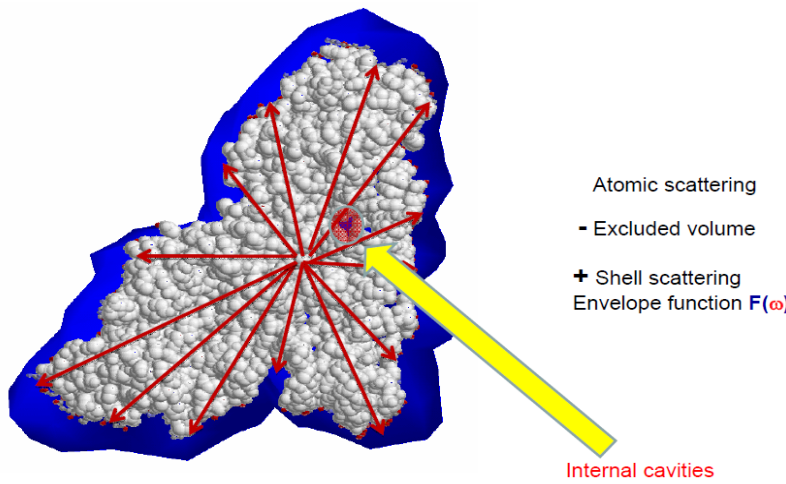

"Gilberto Vlaic" XVII School on Synchrotron Radiation: Fundamentals, Methods and Applications
amenitsch@tugraz.at & amenitsch@elettra.trieste.it
Anorganische CHEMIE

59

Scattering from a macromolecule in solution

$$I(s) = \left\langle |A(s)|^2 \right\rangle_\Omega = \left\langle |A_a(s) - \rho_s E(s) + \delta\rho_b B(s)|^2 \right\rangle_\Omega$$

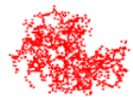

- $A_a(s)$: atomic scattering in vacuum (total scattering length / number of e^-)

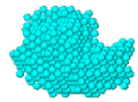

- $E(s)$: scattering from the excluded volume (normalized)

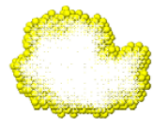

- $B(s)$: scattering from the hydration shell (normalized)

CRYSOL ***(X-rays):*** Svergun et al. (1995). *J. Appl. Cryst.* **28**, 768
CRYSON (***neutrons):*** Svergun et al. (1998) *P.N.A.S. USA*, **95**, 2267

60

Scattering components (lysozyme)

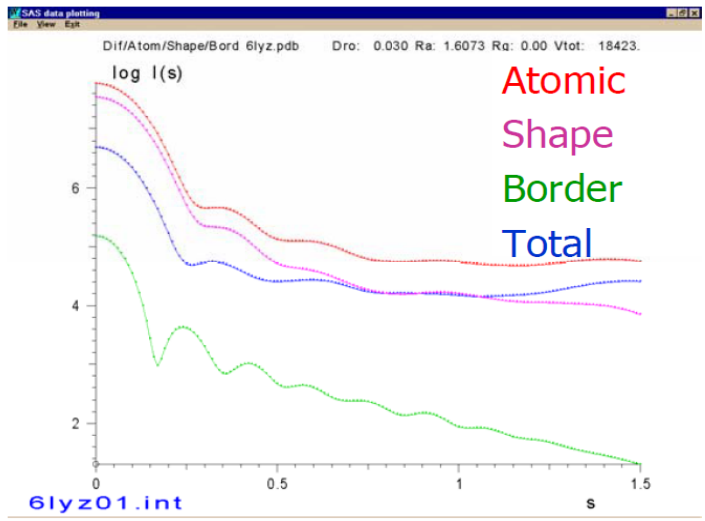

61

amenitsch@tugraz.at &
amenitsch@elettra.trieste.it

SCIENCE • PASSION • TECHNOLOGY

SAXS applications in life science and material science using synchrotron

Heinz Amenitsch
TU-Graz & Austrian SAXS beamine, ELETTRA

Elettra Sincrotrone Trieste

Sample Environment

63

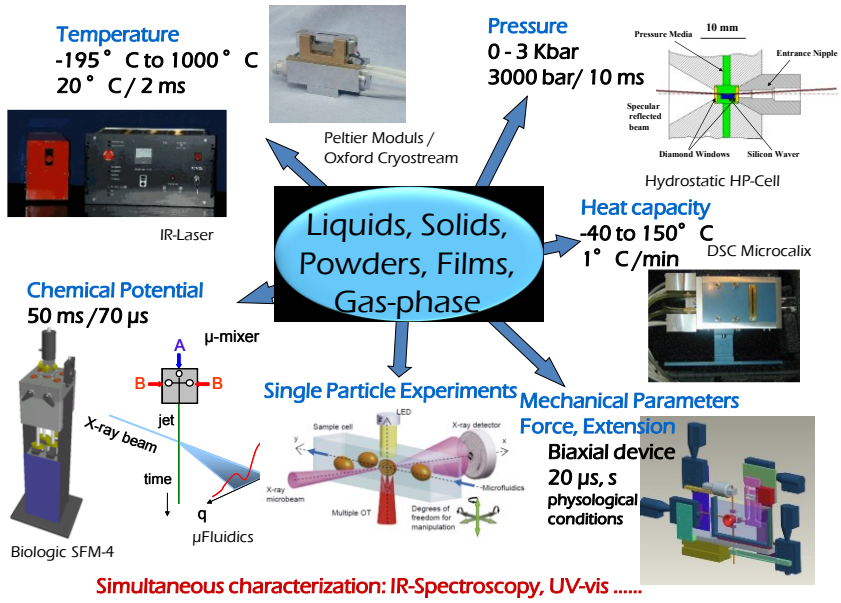

Characterization of carbon nanotube– polyoxometalate electrocatalytic interfaces

64

F.Toma, et al., Nature Chemistry, (2010), 10.1038/NCHEM.761

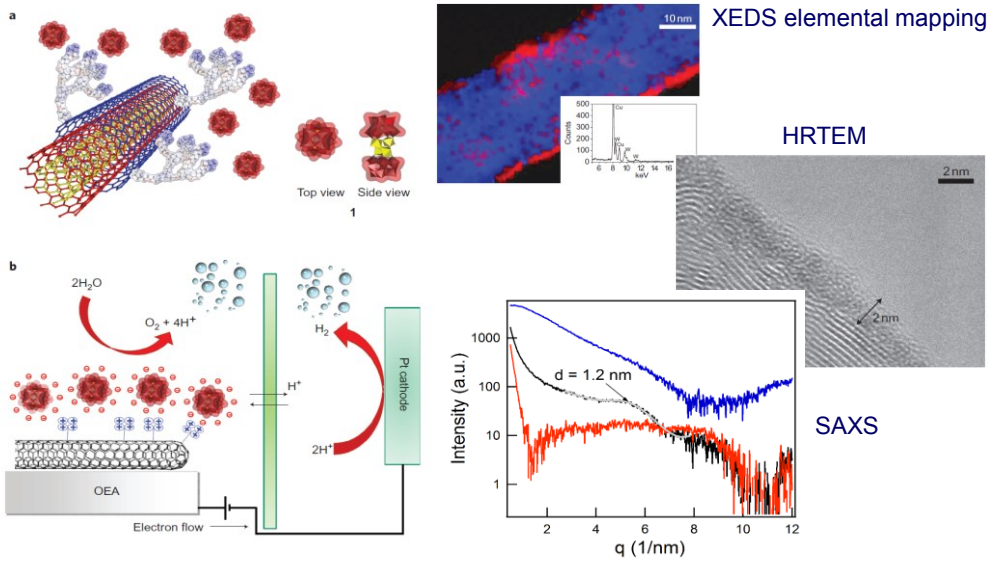

65

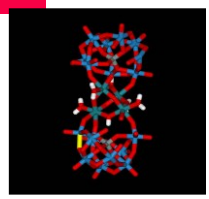

Ru4POM

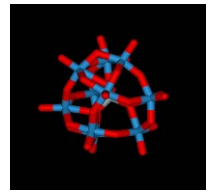

Precursor $SiW_{10}O_{36}$

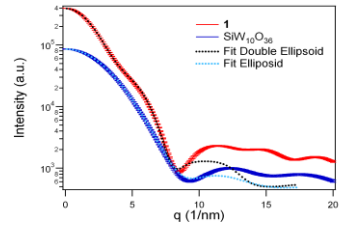

Simulation Crysol ATSAS D.Svergun

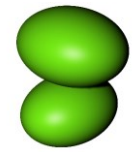

Double ellipsoid model

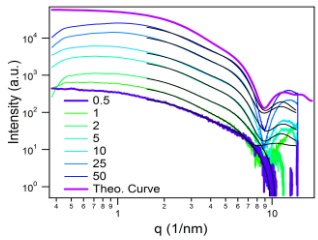

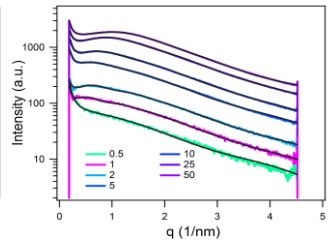

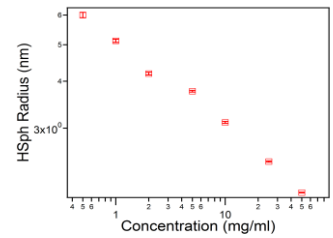

66

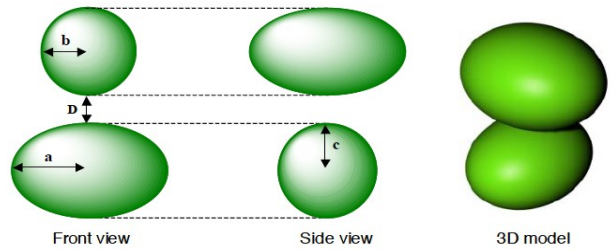

$$I_{scat} = I_0 \cdot \frac{1}{\pi} \int_0^{\pi} d\beta \int_0^{\pi/2} d\alpha \cdot \sin(\alpha) \cdot \frac{1}{4} \cdot F_{2ellip}(q,a,b,c,D,\alpha,\beta)^2 \qquad (1)$$

$$F_{2ellip}(q,a,b,c,R,\alpha,\beta)^2 = \left(F_{ellip}(R_1,q) + F_{ellip}(R_2,q)\right)^2 \cdot \cos\left(q \cdot (D/2+c) \cdot \cos(\alpha)\right)^2 +$$

$$+ \left(F_{ellip}(R_1,q) - F_{ellip}(R_2,q)\right)^2 \cdot \sin\left(q \cdot (D/2+c) \cdot \cos(\alpha)\right)^2$$

$$F_{ellip}(R,q) = 3 \cdot \frac{\sin(q \cdot R) - q \cdot R \cdot \cos(q \cdot R)}{(q \cdot R)^3}$$

$$R_1 = \sqrt{\left(a^2 \cdot \sin(\beta)^2 + b^2 \cdot \cos(\beta)^2\right) \cdot \sin(\alpha)^2 + c^2 \cdot \cos(\alpha)^2}$$

$$R_2 = \sqrt{\left(b^2 \cdot \sin(\beta)^2 + a^2 \cdot \cos(\beta)^2\right) \cdot \sin(\alpha)^2 + c^2 \cdot \cos(\alpha)^2}$$

Artificial Quantasomes for Photo-assisted Water Oxidation

67

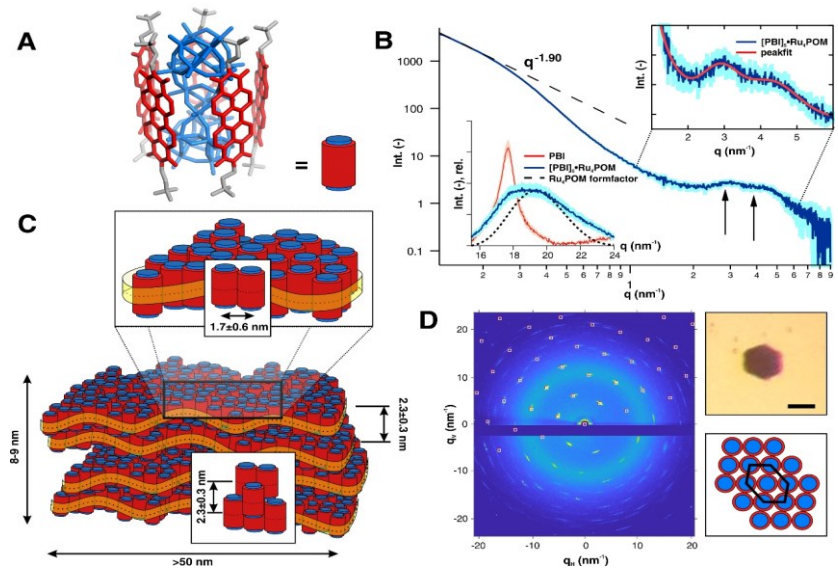

Artificial Quantasomes for Photo-assisted Water Oxidation

68

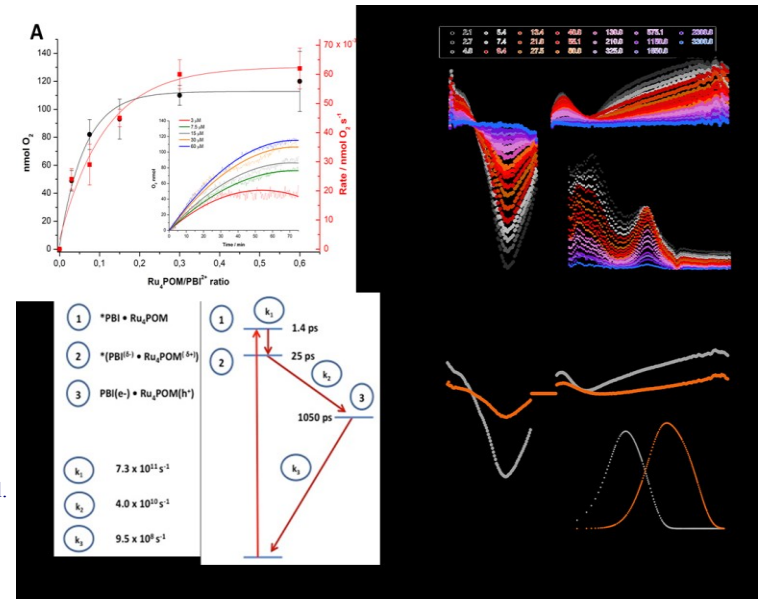

Marcella Bonchio, Zois Syrgiannis, Maurizio Prato et al. Nature Chemistry (2019)

Amphiphilic designer-peptides

69

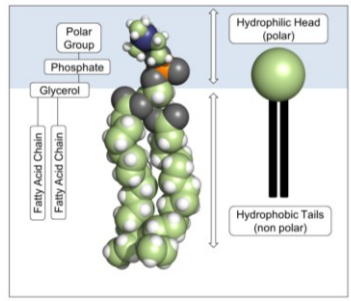

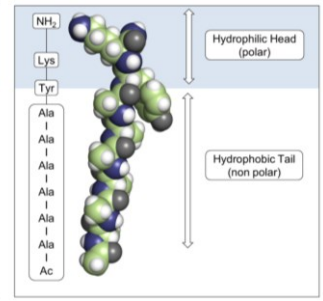

a phospholipid

an amphiphilic designer-peptide

a6yk

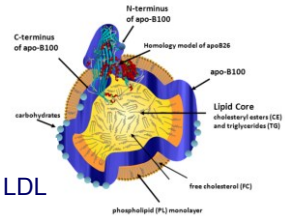

LDL

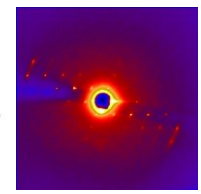

Gazit, E. *Chem. Soc. ReV.* **2007**
Cherny, I.; et al., *Angew. Chem., Int. Ed.* **2008**

Self-assembly

70

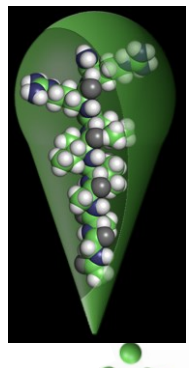

Spherical Micelles
Vesicles
Bilayers

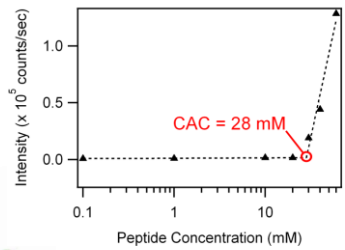

Self-Assembly

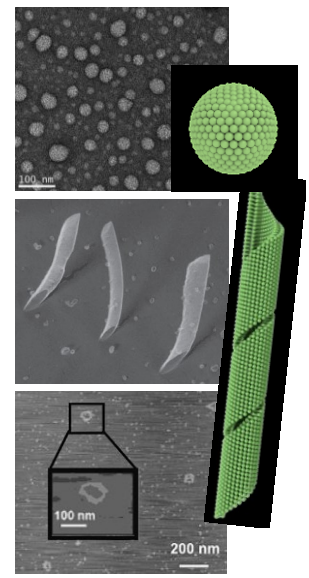

It‘s a double helix!

71

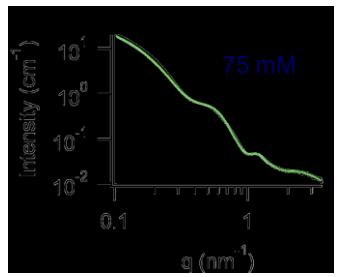

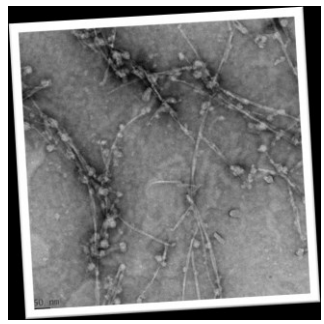

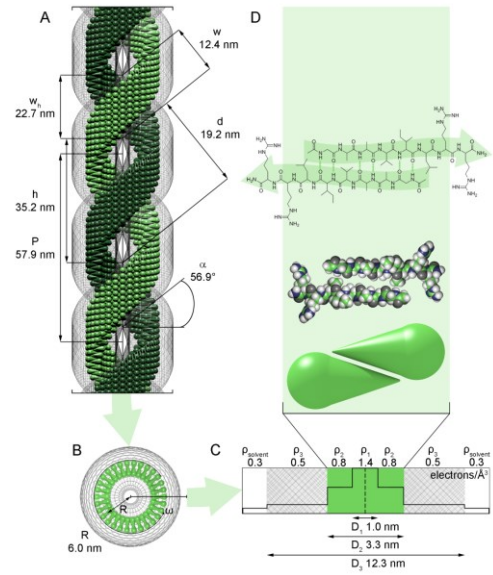

The self-assembly process

72

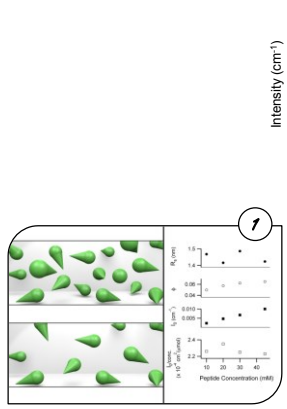

10-45 mM Monomers

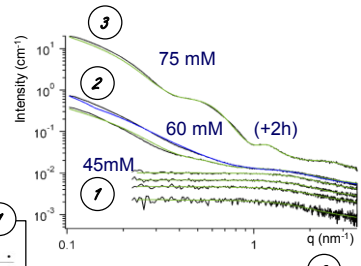

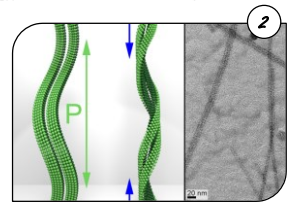

60m M 3-layered single helical tape

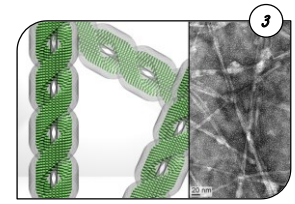

75 mM 3-layered double helical tape

K.Kronmüller et al. sub to JACS (2013)

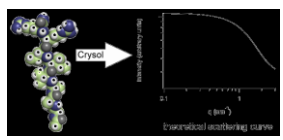

Pontoni D. et al., J. Chem, Phys, 2003
Svergun D.I. et al., J. Appl. Cryst., 1995

SAXS Software Development: SASHEL

73

Ab initio modelling of elongated structures (and globular structures)

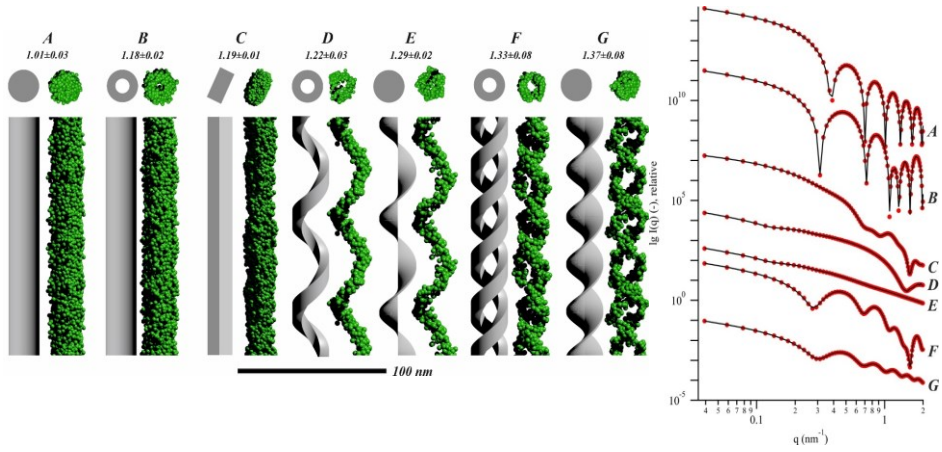

M. Burian , H.A. IUCrJ (2018)

SAXS Software Development: SASHEL

74

Ab initio modelling of elongated structures (and globular structures)

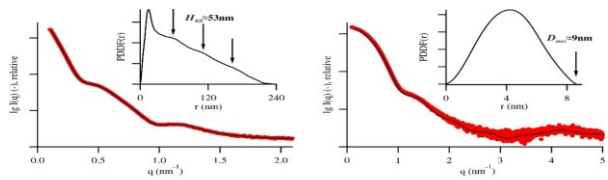

Alcohol Dehydrogenase 1
Valentini E et al., Nucleic Acids Res. **43** (2015)

Kornmueller,K, et al. NanoResearch (2018)

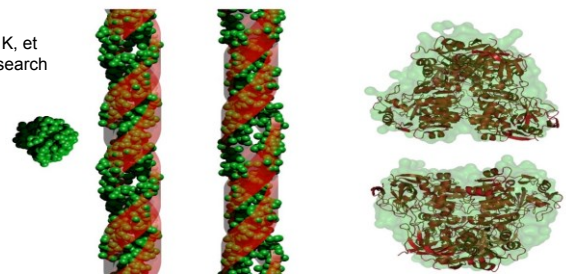

M. Burian , H.A. IUCrJ (2018)

Scanning SAXS - Biomaterials

75

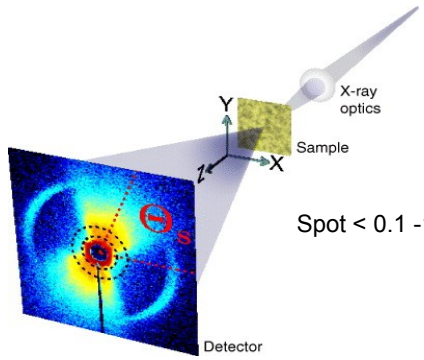

Spot < 0.1 -1 µm

Pic. O.Bunk, et al. New J. Phys. **11** (2009) 123016

Bone

P.Fratzl

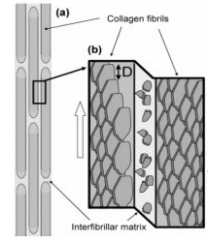

Wood P.Fratzl

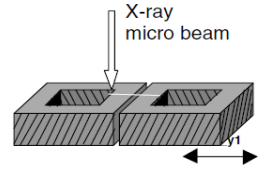

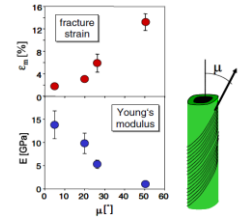

Silica-Sponges, Shells, Tooth, Lobster, Worms, Starch, Eyes……,

Scanning SAXS-Integral Parameters

76

Integated Intensity

$$I = \int_{q\,\min}^{q\,\max} \int_{\chi_1}^{\chi_2} I(q,\chi) q^2 \, \mathrm{d}q \, \mathrm{d}\chi$$

Porod Invariant

$$\tilde{I} = \int I(\mathbf{q}) \, \mathrm{d}^3 q = \int_0^\infty q^2 \, \mathrm{d}q \int_0^\pi \sin\psi \, \mathrm{d}\psi \int_0^{2\pi} I(q,\psi,\chi) \, \mathrm{d}\chi$$
$$= 2\pi^2 \varphi_1 \varphi_2 (\Delta\rho)^2,$$

T-Parameter

$$T = \frac{4}{\pi P} \int_0^\infty I(q) q^2 \, \mathrm{d}q = 4 \frac{\varphi_1 \varphi_2}{\sigma}$$

Porod (1951,1952)

Scanning SAXS - Orientation

77

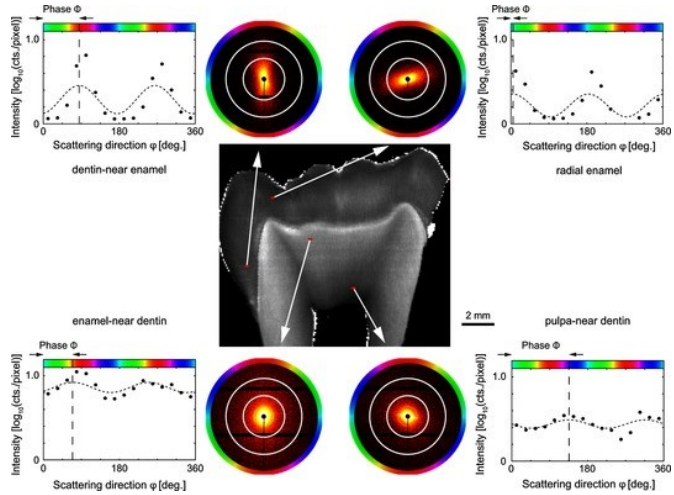

Geiser S. et al., Biointerphases
Journal for the Quantitative Biological Interface Data, 2012

Scanning SAXS - Tooth

78

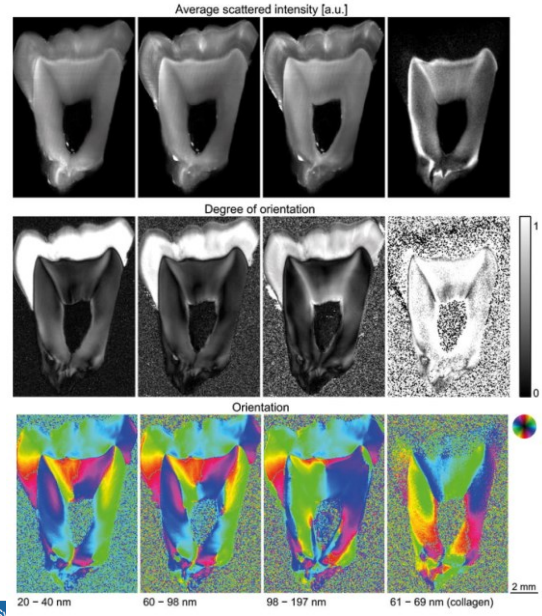

Liposomes and SAXS

79

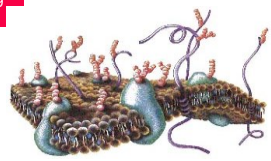

The boundaries of cells are formed by biological membranes, the barriers that define the inside and the outside of a cell.

Phospholipids are the major components of biological membranes that form the structural matrix into which proteins are imbedded.

In aqueous solution: self assembly into, e.g., unilamellar vesicles

Phospholipid Membrane Stack

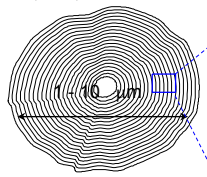

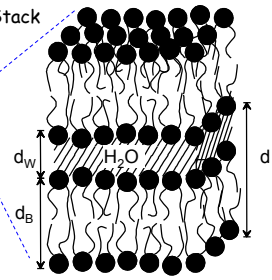

multilamellar vesicle: LIPOSOME

Lyotropic Phases

Bilayer

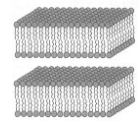

Micelle

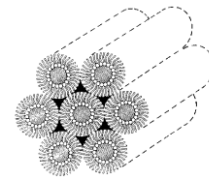

Hexagonal Phase

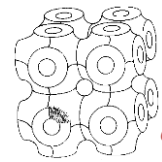

Cubic Phase

Small Angle Scattering - Surface Diffraction

80

Incident beam Scattered beam

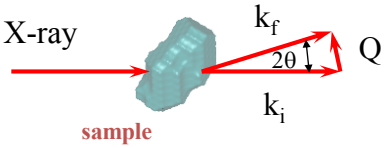

Small-Angle Scattering (Diffraction)

Incident beam Scattered beam

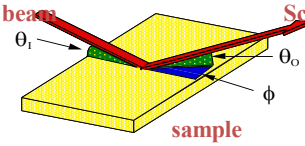

Grazing Incidence Small-Angle Scattering (GISAS) + Reflectometry

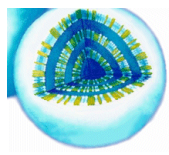

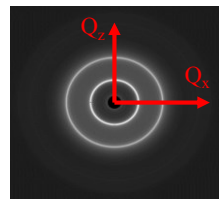

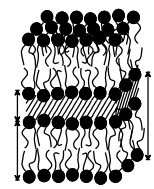

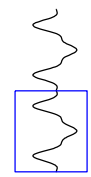

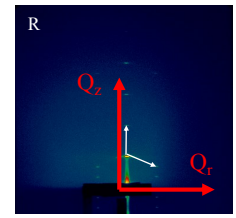

$$I(Q) = \left\langle \left| \int_V d^3r \cdot \rho(\vec{r}) \cdot \exp(-i \cdot \vec{Q} \cdot \vec{r}) \right|^2 \right\rangle \qquad I(Q_z, Q_r) = \left\langle \left| \int_V d^3r \cdot \rho(\vec{r}) \cdot \exp(-i \cdot \vec{Q} \cdot \vec{r}) \right|^2 \right\rangle_r$$

Distorted Wave Born Approximation

81

Vineyard (1982), Shinha et.al. (1988)

$$I(Q_z, Q_r) = |T_i(\alpha_i)|^2 \left\langle \left| \int_V d^3r \cdot \rho(\vec{r}) \cdot \exp(-i \cdot \vec{Q} \cdot \vec{r}) \right|^2 \right\rangle_r |T_f(\alpha_f)|^2$$

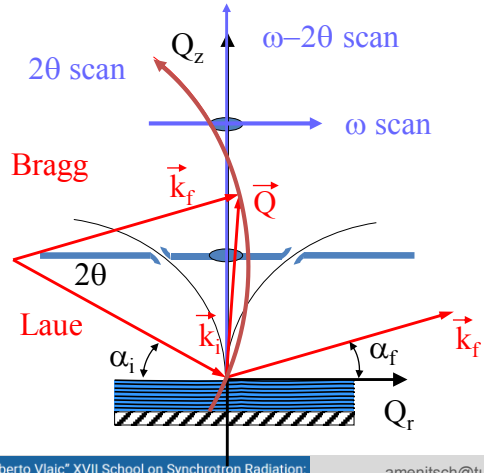

Refraction Effects

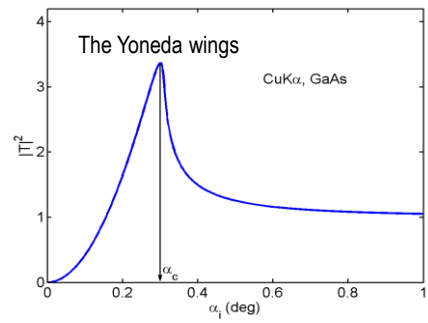

„Higher Orders" of DWBA

82

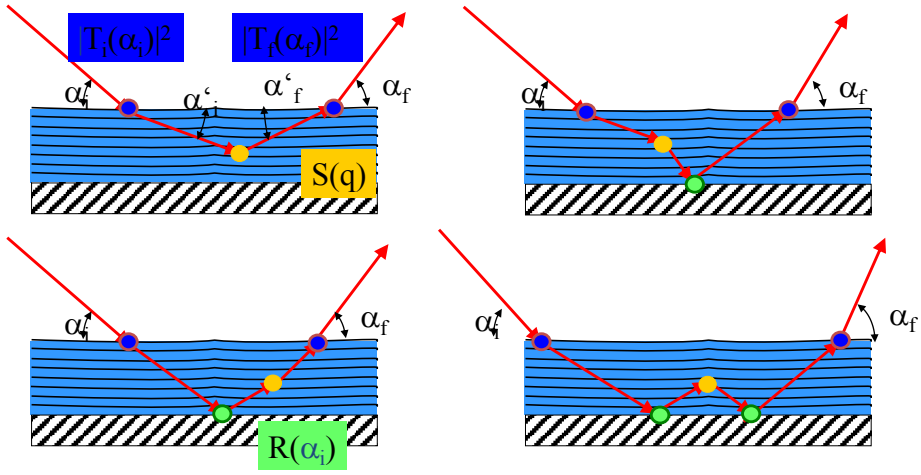

Lazzari R, ISGISAXS: program, J APPL CRYSTALLOGR 35: 406, (2002)
http://www.esrf.fr/computing/scientific/joint_projects/IsGISAXS/isgisaxs.htm
M.P.Tate et al., J.Phys.Chem, 2006

Distorted Wave Born Approximation

83

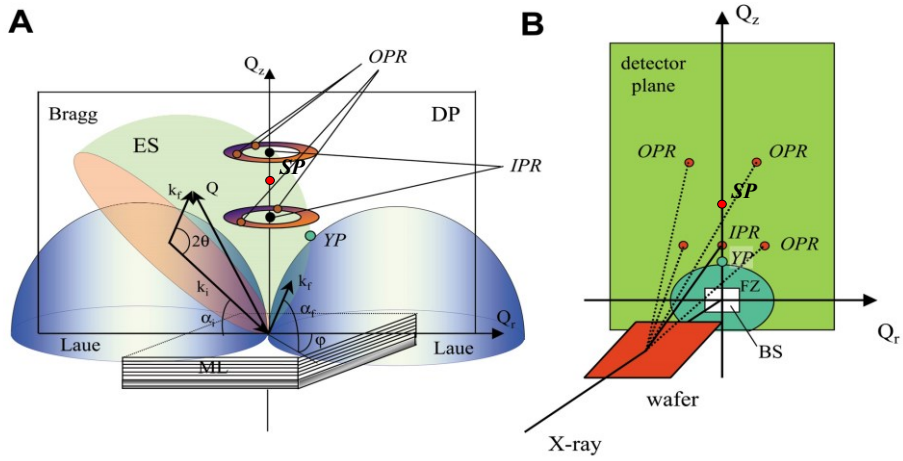

Fig. (A) the scattering geometry in reciprocal space. (B) Scattering geometry in real space. The abbreviations are: (ES) Ewald sphere, (DP) diffraction plane, (OPR) out-of plane reflections, (IPR) in-plane reflections, (ML) multi-layer, (FZ) forbidden zone, (BS) beam stop.

Surface Diffraction Lipids – Rhombohedral Phase

84

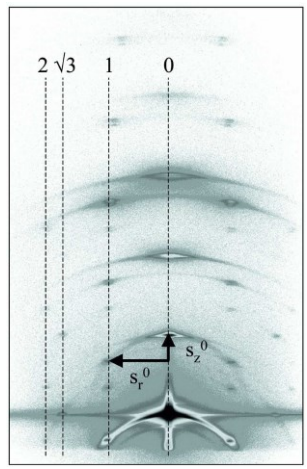

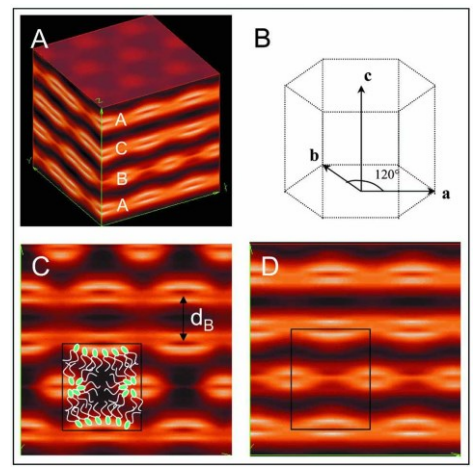

Diffraction Pattern DOPC @ 25° C, 35% rel. humidity

Electron Density Reconstruction: -C DPhPC (d_B= 44.3 Å) -D DOPC (d_B= 48.7 Å), but a= 67 Å / 68 Å

Rappolt,M, et.al., Adv. Coll. and Interf. Science, 111 (2004)

L. Yang, H.W. Huang, Biophys. J. 84 (2003)

What do we learn? Membrane Fusion

85

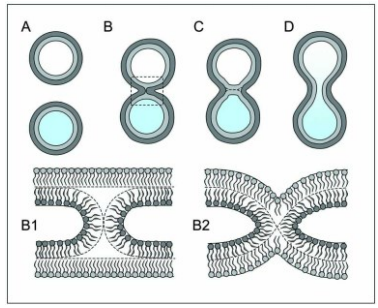

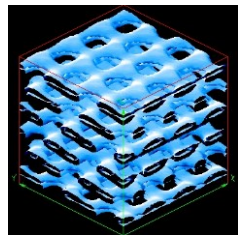

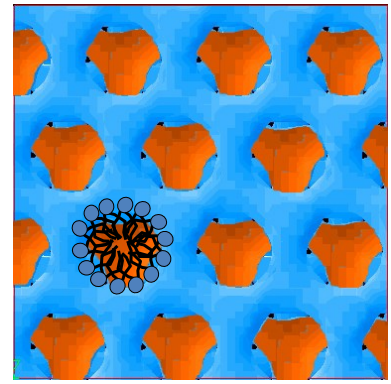

The radius of the torus seems to be confined by the head-group size…

Surface diffraction: Formation of aligned mesoporous thin films

86

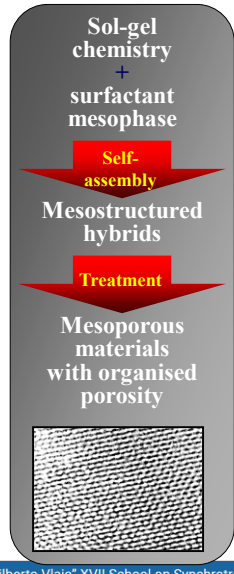

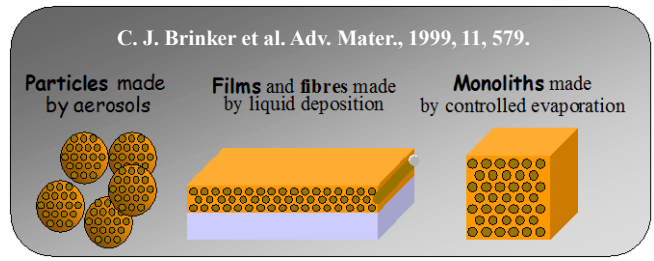

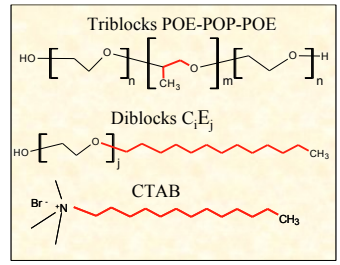

SiO_2 : $Si(OR)_4$
TiO_2 : $TiCl_4$ - $Ti(OR)_4$
ZrO_2 : $ZrCl_4$ - $Zr(OR)_4$
Al_2O_3 : $AlCl_3$
VO_{2-x} : $VOCl_3$
Y_2O_3 : YCl_3
Nb_2O_5 : $NbCl_5$
And binaries systems

The Self-Assembly of thin films as seen by In- Situ SAXS and interferometry

87

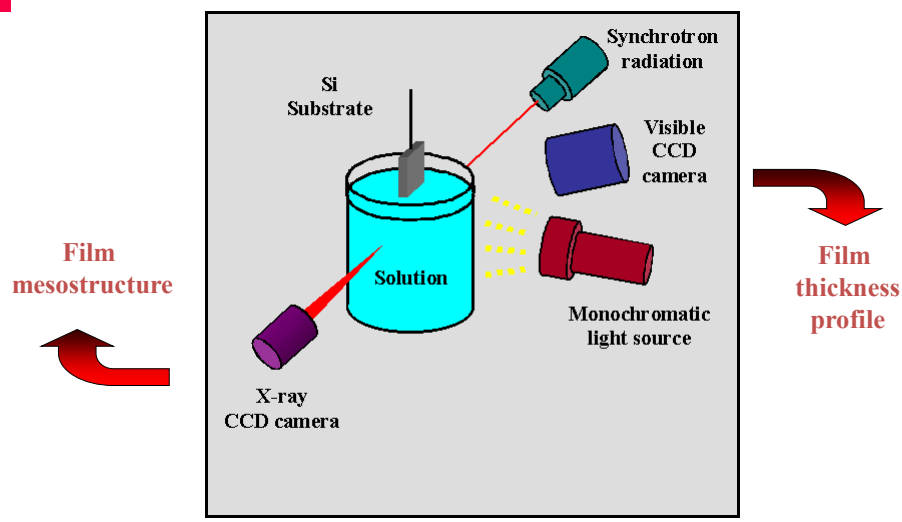

Surface diffraction: Formation of aligned mesoporous thin films

88

CTAB / Si = 0,18
H_2O / Si = 5
HCl / Si = 0.15
Ageing time
Relative Humidity

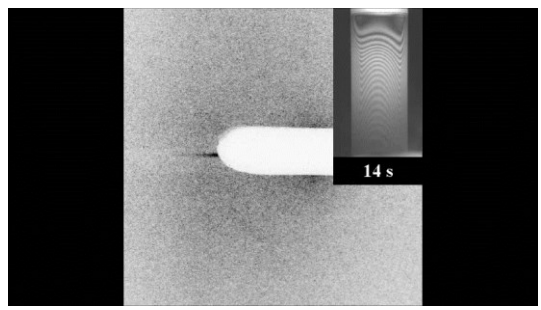

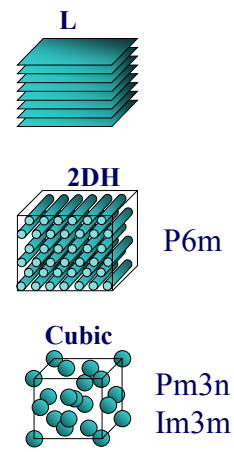

Grosso D, et.al., CHEMISTRY OF MATERIALS *14*, 931,(2002)

The Modulable Steady State

89

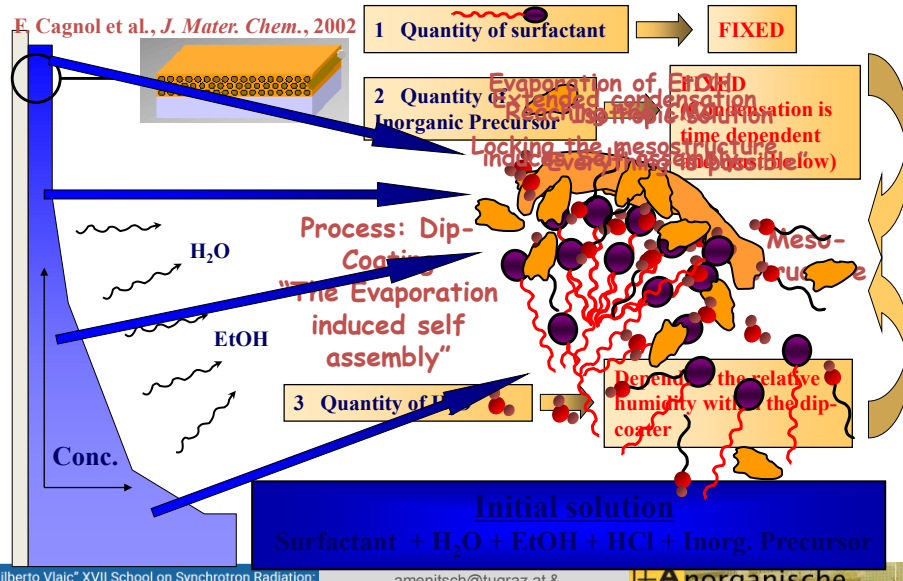

Electrochemistry - GISAXS

90

-Electrochemical GISAXS cell

M.Bogar (CEROP)
P.Wieser

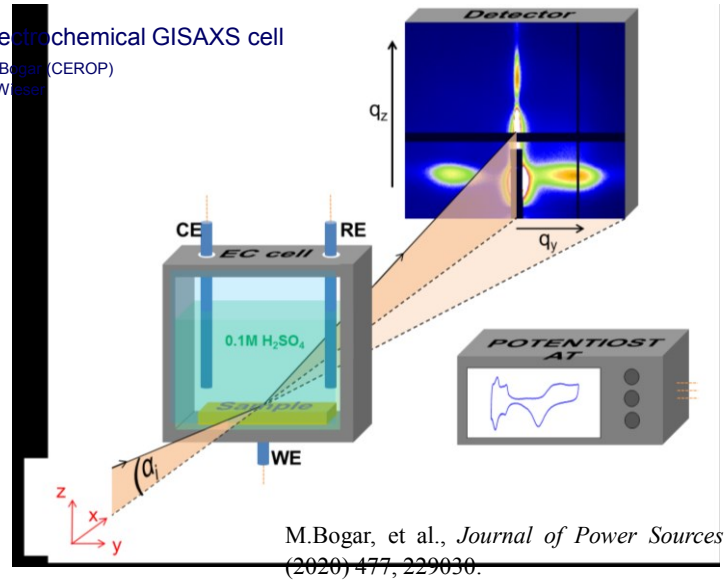

M.Bogar, et al., *Journal of Power Sources* (2020) 477, 229030.

GISAXS: Pt/Ni nanocatalyst fuel cell

91

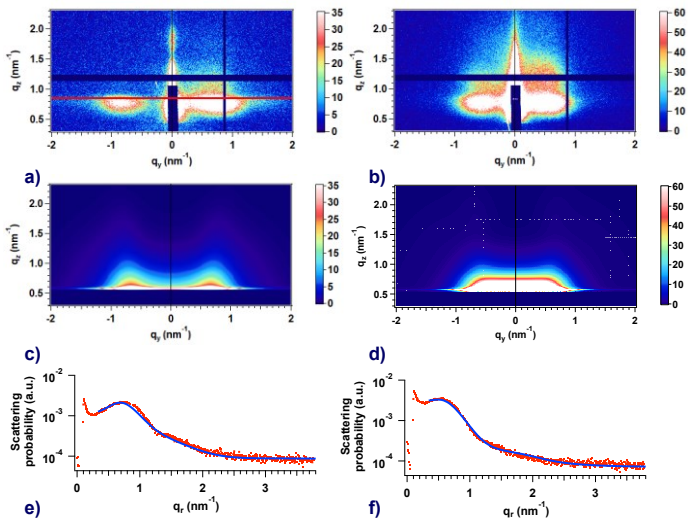

LAYER GEOMETRY:
sandwiched islands

FORM FACTOR:
random spheroid,
H/D constant

SIZE DISTRIBUTION:
Log Norm

STUCTURE FACTOR:
Perkus-Yevick

FORM FACTOR:
D: 4.3 nm
FWHM: 3.7 nm
H/D: 5

STRUCTURE FACTOR:
A/D: 2.95
eta: 0.127

FITGISAXS - D. Babonneau, J.Appl.Cryst, (2010)

GISAXS: Pt/Ni nanocatalyst fuel cell

92

CV# 0 – 1500th

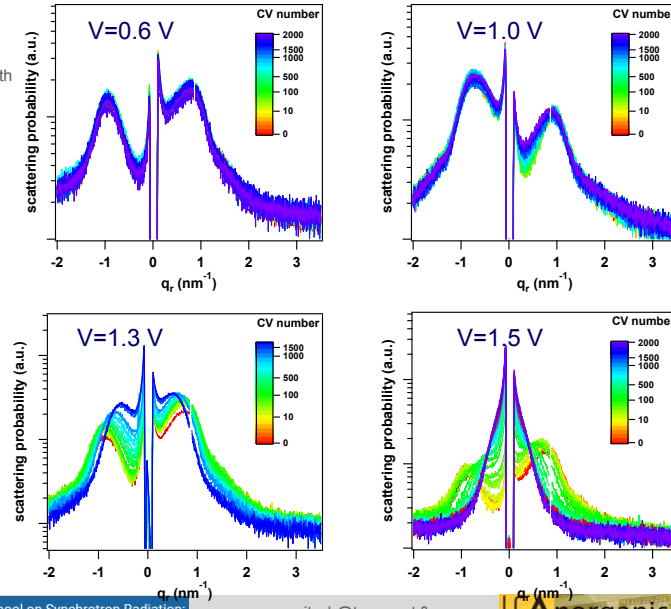

Sketch of the Model - GISAXS: Pt/Ni nanocatalyst

93

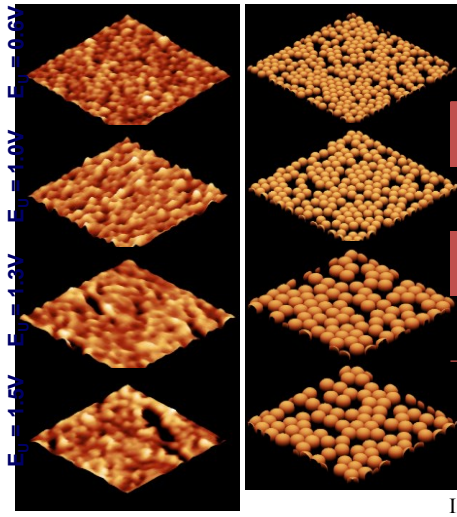

ΔV (V)	R_P (nm)	σ_P (nm)	D_{IP} (nm)
0.6	1.61 ± 0.14	0.56 ± 0.01	6.54 ± 0.04
1.0	1.77 ± 0.06	0.69 ± 0.03	6.50 ± 0.04
1.3	2.52 ± 0.14	0.84 ± 0.06	8.14 ± 0.06
1.5	2.64 ± 0.54	1.55 ± 0.06	14.54 ± 0.06

I. Khalakhan, et al., *ACS Applied Materials and Interfaces* (2020) 12, 17602.

Pt_xNi_{1-x} Dependence - GISAXS: Pt/Ni nanocatalyst

94

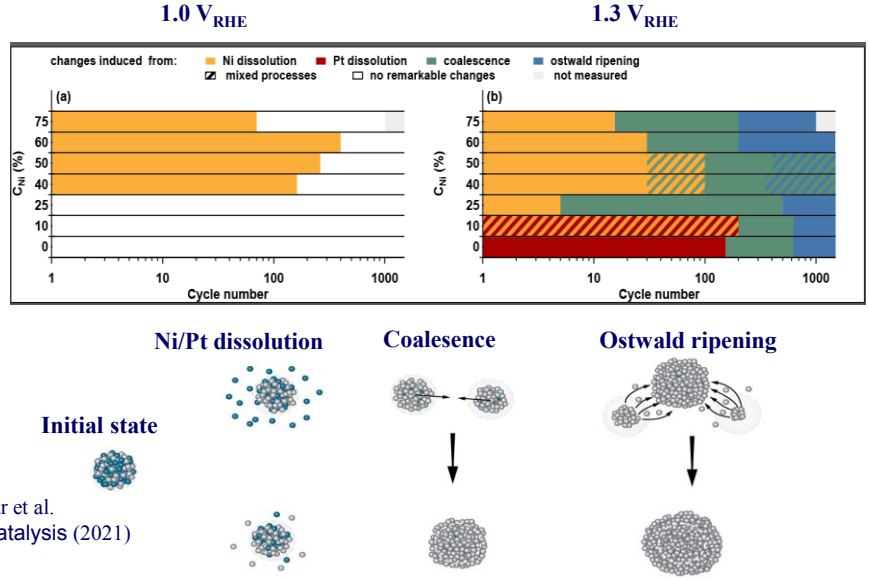

M.Bogar et al.
ACS Catalysis (2021)

Pump Probe: Transient solution scattering

95

Taken from: H.Ihee, et.al. Science **309**, 1233 (2005).

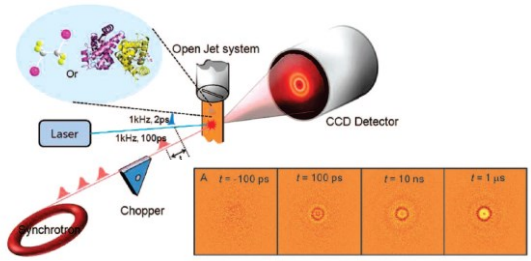

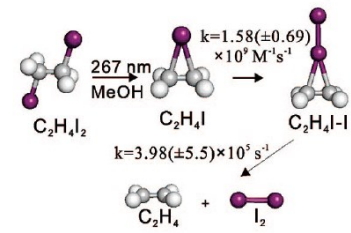

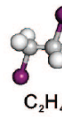

$C_2H_4I_2$

$\lambda_{exc} = 267\ nm$

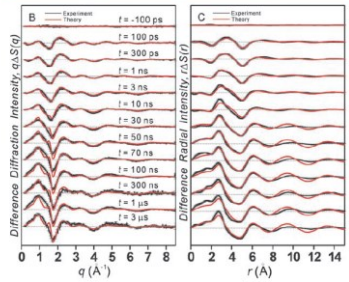

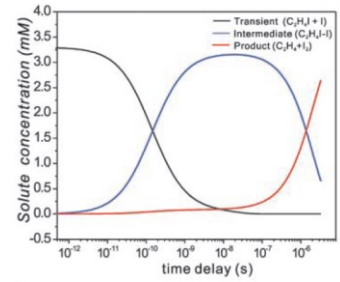

Pump Probe: Implementation

96

Elettra storage ring specifications

- 80 ps x-ray pulses
- 500 MHz cavity -> one pulse every 2ns
- 432 bucket slots -> 864ns circumference time

Cavity signal – hybrid mode:

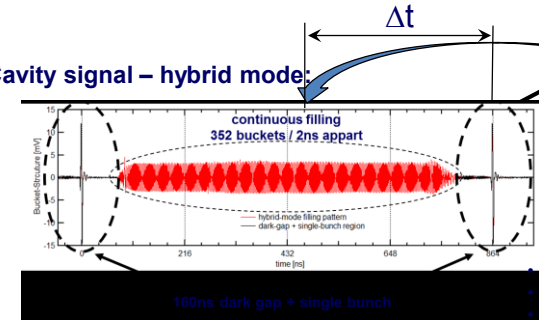

Pharos 20W Nd YAG:Laser

- Pulse width < 230 fs
- Wavelength Harmonics of 1030nm
- Chose-able repetition rate up to 600 kHz
- 100μJ pulses (@1030nm)
- Time-jitter < 5ps

(End September 2018)

PHAROS LIGHT CONVERSION

Pump Probe

97

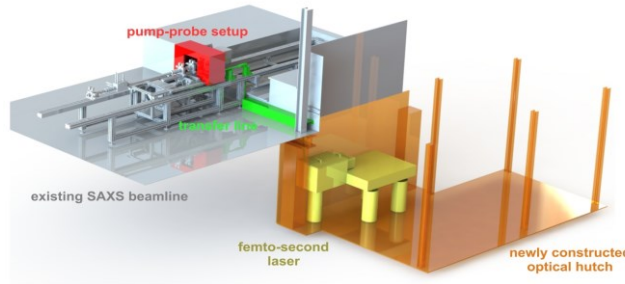

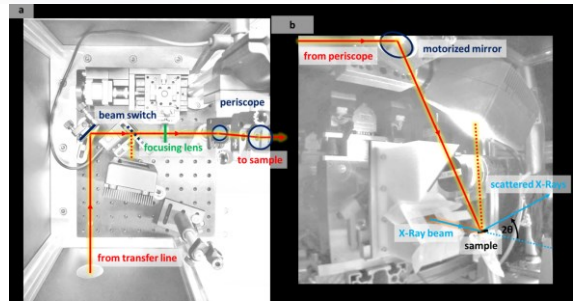

Pump Probe

98

Transient heat-transfer

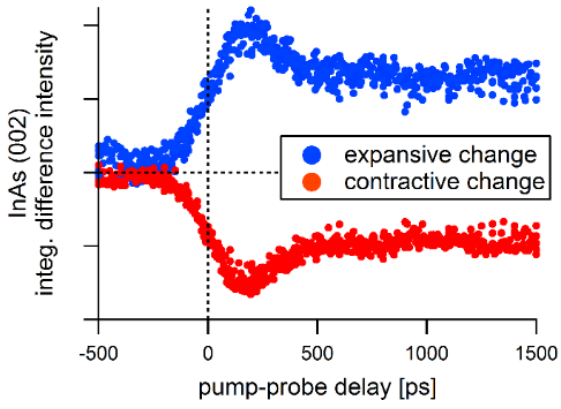

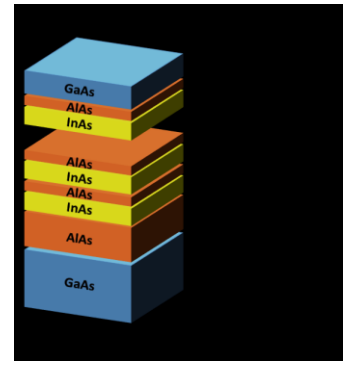

M. Burian, B. Marmiroli, A. Radeticchio, C. Morello, D. Naumenko, G. Biasiol, H. Amenitsch. (2020) J.Appl.Cryst.

Current Science Development – ELETTRA 2.0

99

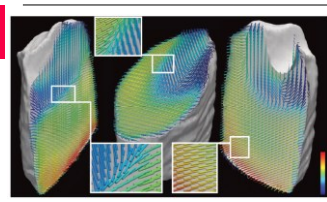

Schaff et al. Nature 2015
3D SAXS tomography tooth PSI
Liebi et al. Nature 2015 PSI
3D SAXS tomography of bone PSI

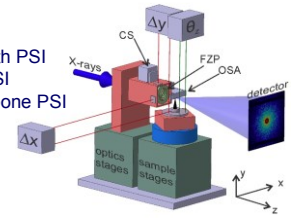

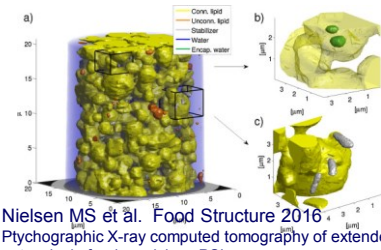

Nielsen MS et al. Food Structure 2016
Ptychographic X-ray computed tomography of extended colloidal networks in food emulsions PSI

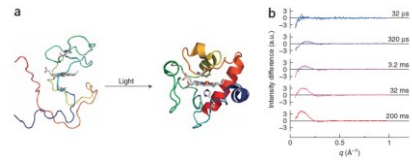

Cammerata M. et al. Nature 2008
Pump probe WAXS Cyt-c. ESRF

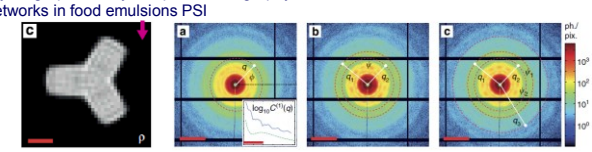

Pedrini et al. Nature com. 2013
2D cross correlation PSI

0.16 1/nm

Conclusion

100

PART I:

-Introduction to the Theory ("Graz School")

-From Experiments to Real Space

-Bio-SAXS ("Hamburg School")

PART II:
-Examples: -Chemistry
-Hierarchical Materials

-Gracing Incidence SAXS ("no school")
-Biomembranes
-*In situ* Chemistry
-*In operando Electrochemistry*
-*Pump-Probe*

www.elettra.eu YouTube SAXS & CERIC-ERIC